Received XX Month, XXXX; revised XX Month, XXXX; accepted XX Month, XXXX; Date of publication XX Month, XXXX; date of current version 11 January, 2024.

Digital Object Identifier 10.1109/OJCOMS.2024.011100

Transmit Power-Efficient Beamforming Design for Integrated Sensing and Backscatter Communication

Shayan Zargari[1], Diluka Galappaththige[1] (*Member, IEEE*), and Chintha Tellambura[1] (*Fellow, IEEE*)

[1]Department of Electrical and Computer Engineering, University of Alberta, Edmonton, AB, T6G 1H9, Canada

CORRESPONDING AUTHOR: Shayan Zargari (e-mail: zargari@ualberta.ca).

ABSTRACT Ambient Internet of Things networks use low-cost, low-power backscatter tags in various applications, and sensing is necessary to introduce perceptive intelligence to the network. In this work, an integrated sensing and backscatter communication (ISABC) system is thus introduced, comprising multiple backscatter tags, a user (reader), and a full-duplex base station (BS) with integrated sensing and communication (ISAC). The BS simultaneously detects backscatter tags and communicates with the user using the same time and frequency resources. The tag-reflected signals provide data to the user and allow the BS to sense the tags' state information. The communication rates for both the user and tags and the BS sensing rate are derived. To minimize the total BS transmit power, the BS communication beamformer, sensing signal, tags' reflection coefficients, and sensing combiners are jointly optimized using the alternating optimization technique. Closed-form solutions are provided for the sensing combiners, while semi-definite relaxation is applied to the BS communication beamformer and sensing signal, and slack optimization is used for the tags' reflection coefficients. For instance, with ten BS antennas, ISABC achieves a 75% gain in combined communication and sensing rates compared to traditional backscatter, with only a 3.4% increase in transmit power. Additionally, ISABC with active tags requires just a 0.24% increase in power compared to conventional ISAC systems.

INDEX TERMS Backscatter communication (BackCom), Integrated sensing and communication (ISAC), Passive tags.

I. INTRODUCTION

INTEGRATED sensing and communication (ISAC) represents a paradigm shift from traditional network models, allowing concurrent sensing (radar) and communication tasks [1]–[3]. Thus, ISAC seamlessly integrates these functions, which carry substantial implications for transitioning beyond fifth-generation (5G) into the domain of sixth-generation (6G) [1]–[3]. Consequently, ISAC devices communicate and sense environmental/state information of targets to facilitate innovative services like precise localization, activity tracking, object detection, urban traffic monitoring, and weather observations [1]–[3].

The 3rd Generation Partnership Project (3GPP) is developing ambient Internet-of-Things (IoT) networks that offer low-power, wireless connectivity, and sensing capabilities [4]. These networks enable data sensing, collection, and sharing for applications in smart homes, autonomous vehicles, healthcare, and more [5]–[8]. In such applications, sensor state information, such as range, direction, and velocity, is essential for tracking, identification, and environment mapping [1]. A promising technique for enabling ambient IoT is symbiotic radio (SR) networks [9], [10].

SR networks use tags that reflect ambient radio frequency (RF) signals from a cellular base station (BS), TV tower, or Wi-Fi access points for data communication [9]–[11]. However, SR differs from conventional ambient backscatter (BackCom) because it employs a common receiver (i.e., a reader or mobile user)to decode both primary legacy and secondary backscatter systems [9], [10]. In contrast, the BackCom reader treats the legacy signal as interference. The SR reader, however, first decodes the primary signal, cancels its effect from the received signal, and then decodes the tag signals.

The use of backscatter tags in an SR network offers several advantages. These tags, which lack active RF components, communicate with a reader by modulating and reflecting

TABLE 1: A comparison between ISABC and the derivatives of ISAC.

Features	**ISAC**	**ISABC**	**ISAC+BackCom**
Target	✓	×	✓
Tag	×	✓	✓
Target's role	Sensing	–	Sensing
Tag's role	–	Communication or C&S	Communication
Additional data at the user	×	✓	×
Power allocation at the BS	✓	✓	✓
User decoding	Conventional	SIC	Conventional
Sensing signal	Passive	Active	Passive

C&S - Communication and sensing.

external RF signals while harvesting energy from them to power their operations [5]–[8]. This method addresses the limitations of battery-powered IoT devices, such as frequent recharging or replacement, which result in high maintenance costs, environmental concerns, and safety risks in industries like power and petroleum. Batteryless backscatter devices (passive tags) or those with limited energy storage (semi-passive tags) effectively mitigate these issues, enabling future IoT networks and applications [5]–[7].

A. Integrated Sensing and Backscatter Communications

Although such ambient IoT devices benefit from low power consumption, sensing capabilities are essential for applications like tracking and environmental mapping in smart homes and warehouses [1]. In a smart home, for example, a tag can act as a sensor, providing background information to the BS. The BS analyzes signals reflected by the tag to estimate parameters for efficient tracking and monitoring, while the tag modulates its data and transmits it to the reader for communication.

In this context, [12] has introduced *integrated sensing and backscatter communications (ISABC)*, which leverages BackCom to enable simultaneous sensing and communication in ambient power-enabled IoT networks. This approach offers an efficient solution for optimizing resource use while addressing the dual sensing and communication tasks.

However, ISABC differs from conventional ISAC systems and integrated ISAC and BackCom, where tags serve communication only. These differences are highlighted in Table 1. Specifically, ISABC replaces traditional ISAC sensing or radar targets with backscatter tags. These enable opportunistic sensing, which leverages unintentionally reflected signals, to estimate state parameters [13]. Hence, ISABC tags transmit data to the reader (or user), and simultaneously, the BS extracts state information about the tags. Conversely, ISAC utilizes targets for sensing, and targets do not carry communication data, whereas ISAC+BackCom uses targets for sensing and tags for communication.

Both BackCom and radar/sensing systems rely on reflected signals for data detection/decoding and target detection, respectively, creating a direct relationship between backscattering and radar functions. The shared characteristics and parameters of the reflected signal can enhance the efficient use of system resources. In particular, load-modulated backscatter signals behave exactly like pulse radar signals [5], [14].

For example, radar systems use reflected echo signals to extract target attributes such as position and velocity. In contrast, backscatter systems use reflected, load-modulated signals to transmit data to a receiver [5], [14]. Each method relies on analyzing echo signals, and none requires an active transmitter at the targets/tags. Both reflected/echo signals are vulnerable to multi-path propagation, interference, and double path loss [5], [14]. Importantly, they can benefit from standard signal processing techniques (e.g., Doppler analysis, angle-of-arrival estimation) for communication and sensing [5], [14]. Thus, ISABC systems exploit these shared characteristics to leverage the same reflected signal for simultaneous data communication and tag detection.

Additionally, both systems employ mono-static and bi-static topologies, making deployment in practical systems and integration into existing systems more feasible. These similarities at the signal and topological levels prompt the exploration of the potential advantages of ISABC [12], [15]. For instance, one can envision extracting tags' state parameters from backscattered signals carrying data. These parameters include a tag's range, angle, velocity, and others. Their estimation can be done by exploiting the properties of tags' reflected signal, such as time of arrival (ToA), angle of arrival (AoA), angle of departure (AoD), time difference of arrival (TDoA), received signal strength (RSS), and Doppler frequency/shifts [13], [15]. In traditional radar, these estimation parameters are called 'radar tracks.'

However, several signal-processing techniques may be needed to harness sensing and backscatter data. For example, the BS or reader/user needs self-interference (SI) cancellation and successive interference cancellation (SIC) techniques [5], [16]. Moreover, such signal processing techniques eliminated the need for passive tags to be physically modified. That implies that passive tags' cost and complexity advantages for IoT networks are preserved.

B. Tag versus Targets

In conventional ISAC systems, targets are external objects (e.g., vehicles, animals, people) that cannot transmit or receive signals. Instead, they reflect incident electromagnetic

(EM) waves, enabling sensing. This falls under the device-free ISAC category. In contrast, backscatter tags are network-registered devices (e.g., sensors) capable of modulating and reflecting incident EM waves, embedding additional data. These tags belong to the device-based ISAC category, where sensing depends on their transmission/reception capabilities, as seen in wireless-based localization for mobile devices. While targets only support sensing, tags can facilitate either (backscatter) communication or both communication and sensing simultaneously.

C. Role of Sensing in BackCom

Integrating sensing into BackCom systems, i.e., ISABC, facilitates the network to extract state information about tags through the same reflected signals used for communication [12]. Such IoT tags are compact with a small form factor and low power and have low-processing capabilities [17], [18]. Thus, this may remove the need for a dedicated sensing network, saving bandwidth and other resources. Therefore, using the same backscattered/antenna reflected signal (i.e., communication signal) for state information extraction enables opportunistic sensing in ambient-powered (i.e., EH-based) IoT networks [12]. On the other hand, leveraging sensing information, the BS can adapt its beamforming based on real-time tag location and movement, improving signal quality, reducing interference, and enhancing tags' EH efficiency. For instance, our problem formulation (P1) utilizes the previous sensing information, such as tag angle, to design the beamforming at the BS (see Remark 1).

Sensing enables context-aware IoT applications, such as smart homes, health monitoring, and agriculture, which require accurate sensing, high data throughput, low latency, reliability, and energy efficiency [17], [18]. To meet these demands, tags act as passive, low-power sensors, providing the BS with valuable state information for monitoring and tracking movements and activities without dedicated sensors. This results in scalable, low-power ISABC networks, enabling efficient and ubiquitous data collection for large IoT deployments. The simultaneous sensing and communication capability of ISABC, combined with reduced power consumption, makes it ideal for power-efficient applications [17], [18].

D. Problem Statement

Despite their wide application potential, multi-tag ISABC systems pose several unique challenges. These include

(Q1) The reader (or user) must detect the tag signals, which are significantly weaker than direct signals due to the double path loss effect [5]–[7]. Before decoding the tags' data, the user must mitigate direct link interference (DLI) [9].

(Q2) Backscattering causes double path losses and deeper fading in tag signals, resulting in limited communication range ($\leq 6\,\mathrm{m}$), poor data rates ($\leq 1\,\mathrm{bps/Hz}$), and low reliability [5]–[7]. While supporting multiple tags is essential in applications, concurrent tag transmissions generate mutual interference, affecting network performance.

(Q3) Passive tags rely primarily on EH for both internal operation and data modulation [5]–[7]. Thus, tag activation plays a critical role in determining the efficiency and reliability of the system, i.e., the activation threshold is typically around $-20\,\mathrm{dBm}$ [5]–[7]. It directly affects the tags' ability to power up and transmit data under varying energy conditions.

(Q4) ISABC networks must ensure the primary and tags communication requirements and sensing quality at the BS for extracting the tags' state information.

However, these challenges in multi-tag ISABC systems have not been addressed before. Additionally, all prior studies [19]–[24] focus on battery-powered active tags.

This paper addresses these challenges by presenting a BS beamforming design. To address (Q1), the SR paradigm is applied, where a cooperative reader or user decodes the direct link data and eliminates the DLI, enabling the decoding of the tags' data. The BS beamforming design is crucial for (Q2) and (Q3), as it mitigates the double path loss effect and supports multiple access for the tags. It also ensures adequate energy delivery for tag activation and reliable data transmission. To tackle (Q4), our problem formulation (P1) guarantees minimum QoS requirements at each node regarding communication and sensing signal-to-noise-to-interference ratio (SINR).

E. Our Contribution

A multi-tag ISABC system is developed with a full-duplex (FD) BS and cooperative reader/user (Fig. 1). The design focuses on the BS communication beamformer, $\mathbf{w}$, sensing signal (covariance) $\mathbf{S}$, sensing combiners, $\{\mathbf{u}_k\}_{k=1}^K$, and the tags' reflection coefficients, $\{\alpha_k\}_{k=1}^K$, to minimize the BS transmit power under a set of communication, EH, and sensing constrains (P1) (15a).

The main contributions of this paper can be summarized as follows:

1) The overall objective of this paper is to intertwine sensing into BackCom and to determine the advantages of ISABC. To this end, a network of multiple tags, a user/reader, and an FD BS is analyzed (Fig. 1). The BS manages communication for both the user and the tags. Specifically, the tags reflect the BS signal to communicate with the user. At the same time, the BS exploits the tag reflections to assist the estimation of their state information, such as range, angle, velocity, and others.
2) The specific objective is to optimize BS communication beamformer ($\mathbf{w}$), BS sensing signal ($\mathbf{s}_0$), BS sensing combiners ($\{\mathbf{u}_k\}_{k=1}^K$), and tag power reflection coefficients ($\{\alpha_k\}_{k=1}^K$). The optimization criterion minimizes BS transmit power while ensuring each

node meets its QoS requirements, i.e., communication rates, (i.e., user and tags), sensing rate, and EH thresholds. The resulting problem (P1), (15a), is non-convex and NP-hard due to the existence of products of the optimization variables, and thus widely available convex algorithms cannot solve it.

3) To address this, an AO approach is employed [25]. Initially, the BS sensing combiners are optimized using minimum mean-squared error (MMSE) filtering and the generalized Rayleigh quotient form of the sensing SINR [26], [27]. Subsequently, the BS communication beamformer and sensing signal are optimized using the semidefinite relaxation (SDR) method [28], [29]. Finally, the tag reflection coefficients are optimized via the slack-optimization technique [30]. The cycle repeats until convergence.
4) Convergence and complexity analysis and simulations are provided to assess the efficiency of ISABC, comparing it to conventional ISAC, communication-only, and sensing-only schemes (with/without EH). With a configuration of ten BS antennas each for transmission and reception, ISABC offers a 75% combined communication and sensing rate enhancement compared to the conventional BackCom, while only needing a modest 3.4% rise in transmit power.

F. Related Works

Our previous work [12] was the first to explore the integrated functionalities and resulting performance metrics of a limited ISABC system. In contrast, ISAC and SR systems are **separately** studied in [9], [10], [32]–[38]. Study [12] leverages the synergistic potential between ISAC and BackCom. Subsequently, several ISABC studies have been conducted [19]–[24], further expanding on the fundamental concepts introduced [12].

In [12], the integration of sensing at an FD BS with a backscatter tag and a user is detailed. The tag reflects the BS signal to transmit data to the user/reader, while the BS extracts the tag's state information from its backscattered signal. This study provides closed-form expressions for the user communication rate, the tag's BackCom rate, and the sensing rate at the BS. However, it does not address multiple tags, BS communication beamformers, sensing signals, sensing combiners, or tag reflection coefficients beyond a single-tag setup.

Reference [31] exploits the RIS to enhance both sensing and communication in IoT networks. In this system, a BS simultaneously detects backscattered signals from multiple IoT devices and senses targets. The sum rate is maximized by jointly optimizing the BS's transmit beamforming and the RIS reflection coefficients based on fractional programming (FP) and AO algorithms. Reference [39] proposes a system where the RIS functions as a helper or transceiver, addressing energy constraints of IoT devices and enabling non-line-of-sight sensing. Reference [19] studies a backscatter-enabled hybrid RIS-assisted non-orthogonal multiple access (NOMA) network with ISAC capabilities. Part of the RIS operates as a backscatter device, transmitting data to nearby users. At the same time, the rest supports communication between the BS and NOMA users without direct links, with the BS also performing target sensing. This work examines the coexistence of ISAC and backscatter rather than ISABC. In [20], an ISABC system with two NOMA users and a single backscatter tag is analyzed with closed-form expressions for the outage probability, ergodic communication rates, and sensing rates. Reference [21] integrates ISAC into an SR system with bi-static sensing, using RISs as backscatter tags and focusing on channel state information (CSI) estimation through a compressed sensing problem and a 1D AoA sensing algorithm. In [22], [23], a beamforming design for a single-tag, single-user ISABC system is presented with a joint framework for tag detection, estimation, and communication improvement. Reference [24] proposes a zero-force (ZF) beamforming design and a power minimization scheme for a single-tag, single-user ISABC system.

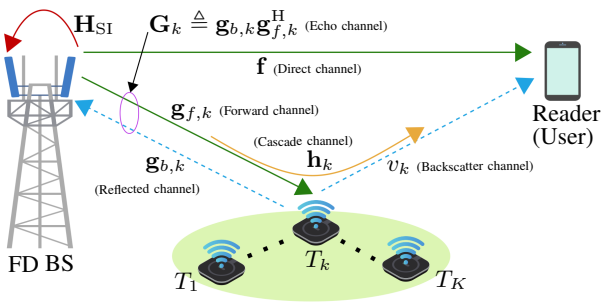

FIGURE 1: An ISABC system setup.

Table 2 provides a summary of relevant works, emphasizing the unique contribution of this paper. The table reveals substantial differences in the system design, problem formulation, and algorithmic approach of each work. The critical contribution of this work is the beamforming design for a multi-tag ISABC system, addressing the challenges (Q1)-(Q4).

Notation: Vectors and matrices are expressed by boldface lower case letters $\mathbf{a}$ and capital letters $\mathbf{A}$, respectively. For a square matrix $\mathbf{A}$, $\mathbf{A}^{\mathrm{H}}$ and $\mathbf{A}^{\mathrm{T}}$ are Hermitian conjugate transpose and transpose of a matrix, respectively. $\mathbf{I}_M$ denotes the M-by-M identity matrix. The Euclidean norm of a complex vector and the absolute value of a complex scalar are denoted by $\|\cdot\|$ and $|\cdot|$, respectively. The distribution of a circularly symmetric complex Gaussian (CSCG) random vector with mean $\boldsymbol{\mu}$ and covariance matrix $\mathbf{C}$ is denoted by $\sim \mathcal{CN}(\boldsymbol{\mu}, \mathbf{C})$. The expectation operator is denoted by $\mathbb{E}[\cdot]$. Besides, $\mathbb{C}^{M\times N}$ and $\mathbb{R}^{M\times 1}$ represent $M \times N$ dimensional complex matrices and $M \times 1$ dimensional real vectors, respectively. Further, $\mathcal{O}$ expresses the big-O notation.

II. System, Channel, and Signal Models

The system, channel, and signal models are described next.

TABLE 2: Summary of related works.

Ref.	FD BS	EH	Tag (Number, Type)	Users	Configuration	Objectives	Algorithms
[19]	✓	✗	Single, RIS	Multiple (NOMA)	ISAC+BackCom	Maximize $\mathcal{R}_b$ and sensing power in a RIS-assisted BackCom	Dynamic user clustering, SCA, AO
[20]	✓	✗	Single, BT	2 (NOMA)	ISABC	Closed-form expressions for outage probability, communication and sensing rates	–
[21]	✗	✗	Multiple, RISs	Single	ISAC+BackCom	Estimating the CSI of the tag channels	CS, sparse Bayesian learning
[22]	✓	✗	Single, BT	Single	ISABC	Joint beamforming for tag detection, estimation, and $\mathcal{R}_c$ maximization	SCA, SDR
[24]	✓	✗	Single, BT	Single	ISABC	Minimize P_t with ZF beamforming	ZF and SOCP
[31]	✗	✗	Multiple, targets	Tags, RISs	ISAC+BackCom	Joint beamforming, RIS phase shifts, receive beamforming design, and $\mathcal{R}_c$ maximization	FP, AO
This paper	✓	✓	Multiple, BT	Single	ISABC	Minimize P_t subject to communication SINR (primary and backscatter), tags' EH, and sensing SINR	SCA, SDR, AO

BT - Backscatter tag. SCA - Successive convex approximation. AO - Alternative optimization. CS - Compressed sensing. SDR - Semidefinite relaxation. SOCP - Second-order cone programming. $\mathcal{R}_b$ - Backscatter (sum) rate. $\mathcal{R}_c$ - Primary (sum) rate. P_t - BS transmit power.

A. System Model

The ISABC network, Fig. 1, has an FD BS with M transmit and N receiver uniform linear array (ULA) antennas, K single-antenna backscatter tags/sensors, denoted by T_k for $k \in \{1, \ldots, K\}$, and a single-antenna user (or mobile reader). The BS antennas are spaced at half-wavelengths [16]. The tags perform EH and backscatter data to the reader.

The BS transmits a signal for ISAC purposes. The tags absorb a part of it for EH and reflect the rest for data communication. A cooperative user decodes BS signal/data and then uses SIC to decode tags' data. The BS also captures the tag-reflected signals and uses them to tags' state information [12], [40]. The BS operates in the FD mode and has separate antennas for transmission and reception to limit SI, assuming perfect cancellation and synchronized timing [40], [41].

B. Communication Channels

Flat-fading block channel models are assumed. During each fading block, the channels between the BS and the user (i.e., direct), the BS and T_k (i.e., forward), and T_k and the user (i.e., backscatter) are denoted by $\mathbf{f} \in \mathbb{C}^{M\times 1}$, $\mathbf{g}_{f,k} \in \mathbb{C}^{M\times 1}$, and $v_k \in \mathbb{C}$, respectively. Moreover, $\mathbf{g}_{b,k} \in \mathbb{C}^{N\times 1}$ is the T_k-to-BS receiver (i.e., reflected channel). Channels $\mathbf{f}$ and v_k are modeled as Rayleigh fading and given by

$$\mathbf{a} = \zeta_a^{1/2}\tilde{\mathbf{a}}, \tag{1}$$

where $\mathbf{a} \in \{\mathbf{f}, v_k\}$. In (1), ζ_a captures the large-scale path loss and shadowing, which stays constant for several coherence intervals. Moreover, $\tilde{\mathbf{a}} \sim \mathcal{CN}(\mathbf{0}, \mathbf{I}_A)$ accounts for the small-scale Rayleigh fading[1], where $A \in \{M, 1\}$. Moreover, the cascaded channel between the BS and reader through T_k, i.e., BS-T_k-user, is denoted as $\mathbf{h}_k = \mathbf{g}_{f,k}(\theta_k)v_k$ for $k \in \{1, \ldots, K\}$.

[1]Note that $v_k = \zeta_{v_k}^{1/2}\tilde{v}_k$ and $\tilde{v}_k \sim \mathcal{CN}(0, 1)$.

C. Sensing Channel Model

To model the interaction between the BS and the backscatter tag, the tag is treated as a single-point reflector [16], an assumption typical in radar and communication systems. Specifically, the paths between the BS and the tag are described by a line-of-sight (LoS) channel. In this scenario, the tag is far enough from the BS that its reflection properties can be fully characterized by a single azimuth angle and a reflection coefficient (path loss) [40], [42]. The transmit/receiver array steering vector to the direction θ_k is given by

$$\mathbf{b}(\theta_k) = \sqrt{\frac{\zeta_b}{B}}\left[1, e^{j\pi\sin(\theta_k)}, \ldots, e^{j\pi(B-1)\sin(\theta_k)}\right]^{\mathrm{T}}, \tag{2}$$

where $\mathbf{b} \in \{\mathbf{g}_{f,k}, \mathbf{g}_{b,k}\}$, $B \in \{M, N\}$, θ_k is the direction of T_k for the BS and user/reader direction, and ζ_b is the path loss. Equal arrival and departure angles are assumed for the target. Also, it is important to note that if the target is static or moving slowly, the beamforming solution will also change gradually. In such cases, using an estimated or predicted direction for the target is often sufficient for designing the beamforming strategy. Therefore, for the optimization problem, angle θ_k remains constant.

On the other hand, ζ_b accounts for the path loss and captures the signal attenuation over distance. Then, the effective sensing channel between the BS and T_k is given by [42]:

$$\mathbf{G}_k \triangleq \mathbf{g}_{b,k}(\theta_k)\mathbf{g}_{f,k}^{\mathrm{H}}(\theta_k). \tag{3}$$

Here, $\mathbf{G}_k$ captures the complex amplitude of the k-th target (i.e., T_k), including the effective path loss, channel fading, and distance and directional information of the target [42].

D. SI Channel Model

The SI channel between the transmitter and the receiver of the BS is denoted as $\mathbf{H}_{\mathrm{SI}} \in \mathbb{C}^{M\times N}$.

In typical BackCom applications, tags are often deployed in stable environments such as rooms or warehouse shelves, maintaining a clear LoS to the BS. This setup supports applications like inventory tracking and smart shelving [5]–[8]. Note that the communication links, including BS-user and tags-user connections, encounter various propagation challenges due to mobility, obstacles, and varying distances. Hence, the Rayleigh fading model is commonly employed due to its stochastic nature, effectively capturing the diverse signal paths encountered in urban landscapes [12], [16], [43], [44]. However, the proposed optimization framework is adaptable to any fading model. Additionally, performance trends remain relatively consistent across different fading models (Fig. 10).

E. Tag's EH Model

Passive tags do not generate RF signals. Thus, their power consumption is ultra-low, and they can operate without batteries and rely entirely on EH. They transmit their data by simply reflecting (i.e., backscattering) an external RF signal. They simultaneously communicate data and perform EH by power-splitting the incident RF signal [45], [46].

The power-splitting operation can be described as follows: let the incident RF power at tag T_k be p_k^{in}. The tag reflects a fraction of p_k^{in} and harvests the remainder [45], [46]. These amounts can be quantified as follows.

1) The reflected power used for data transmission is $\alpha_k p_k^{\text{in}}$, where α_k is T_k's reflection coefficient.
2) The harvested power, p_k^{h}, can be modeled as a linear or nonlinear function of p_k^{in}. The linear model estimates the harvested power at each tag as $p_k^{\text{h}} = \eta(1-\alpha_k)p_k^{\text{in}}$, where $\eta \in (0,1]$ is the power conversion efficiency. Although the linear model is the most widely used in the literature due to its simplicity, it ignores the nonlinear characteristics of actual EH circuits, such as saturation and sensitivity [45], [46].

Consequently, a parametric nonlinear sigmoid EH has been widely used [46]. It models the total harvested power at T_k as $p_k^{\text{h}} = \Phi((1-\alpha_k)p_k^{\text{in}})$, where $\Phi(\cdot)$ is a function representing nonlinear effects [46, eq. (4)].

Regardless of the choice of a linear or nonlinear model, the activation threshold, i.e., p_b, is the critical parameter. It is the minimal power required to wake up the EH circuit, which is typically $-20\,\text{dBm}$ for commercial passive tags [6]. Thus, to activate the tag, the harvested power should exceed the threshold, i.e., $p_k^{\text{h}} \geq p_b$. In particular, $(1-\alpha_k)p_k^{\text{in}} \geq p_b'$, where $p_b' \triangleq \Phi^{-1}(p_b)$ and $\Phi^{-1}(p_b) = b_{\text{NL}} - \frac{1}{a_{\text{NL}}}\ln\left(\frac{M_{\text{NL}}-p_b}{p_b}\right)$. Parameters a_{NL} and b_{NL} represent circuit characteristics like capacitance and resistance. M_{NL} is the maximum harvested power when the EH circuit is saturated. Parameters a_{NL}, b_{NL}, and M_{NL} can be derived using a curve fitting tool [46]. Without loss of generality, the nonlinear EH model is adopted for the rest of this paper.

F. Transmission Model

The BS transmits the signal $\mathbf{x} \in \mathbb{C}^{M\times 1}$, which includes both communication and sensing components, given by

$$\mathbf{x} = \mathbf{w}x_d + \mathbf{s}_0, \tag{4}$$

where $x_d \in \mathbb{C}$ is the data symbol for the user/reader with unit power, i.e., $\mathbb{E}\{|x_d|^2\} = 1$, $\mathbf{w} \in \mathbb{C}^{M\times 1}$ is the BS communication beamformer associated with the user and the tag (backscattering), and $\mathbf{s}_0 \in \mathbb{C}^{M\times 1}$ is the dedicated sensing signal with covariance matrix $\mathbf{S} \triangleq \mathbb{E}\{\mathbf{s}_0\mathbf{s}_0^{\text{H}}\}$ [16]. Covariance $\mathbf{S}$ is designed to increase the degrees of freedom of the transmit signal to enhance sensing performance. To this end, $\mathbf{s}_0$ is chosen as the eigenvector of the maximum eigenvalue of $\mathbf{S}$ [47]. It is also assumed that x_d and $\mathbf{s}_0$ are independent of each other [16].

The user receives the BS signal and the tags' backscattered signals. The propagation delay differences for all signals are assumed to be negligible [9]. The user-received signal is thus given by

$$y = \underbrace{\mathbf{f}^{\text{H}}(\mathbf{w}x_d + \mathbf{s}_0)}_{\text{Direct signal}} + \underbrace{\sum_{k=1}^{K}\sqrt{\alpha_k}\mathbf{h}_k^{\text{H}}(\mathbf{w}x_d + \mathbf{s}_0)c_k}_{\text{Tag signals}} + \underbrace{z_u}_{\text{AWGN}}, \tag{5}$$

where $z_u \sim \mathcal{CN}(0,\sigma^2)$ is the additive white Gaussian noise (AWGN) at the user with 0 mean and σ^2 variance, $\mathbf{h}_k$ is the effective backscatter channel through T_k, i.e., $\mathbf{h}_k = \mathbf{g}_{f,k}(\theta_k)v_k$, and c_k is T_k's data with $\mathbb{E}\{|c_k|^2\} = 1$. As the user/reader and BS constitute the primary network, the sensing signal, $\mathbf{s}_0$, can be exchanged via a control link [48]. It is thus assumed that the user knows $\mathbf{s}_0$ in advance and removes $\mathbf{f}^{\text{H}}\mathbf{s}_0$ before decoding data. The user-received signal can then be expressed as

$$y = \underbrace{\mathbf{f}^{\text{H}}\mathbf{w}x_d}_{\text{Desired signal}} + \sum_{k=1}^{K}\sqrt{\alpha_k}\mathbf{h}_k^{\text{H}}\left(\mathbf{w}x_d + \mathbf{s}_0\right)c_k + z_u. \tag{6}$$

Next, the user performs SIC to recover the secondary data from the tags. Specifically, the user first decodes x_d by treating tag signals as interference. The desired signal is subtracted from the received signal (6) for decoding the tags' data. The post-processed signal for decoding c_k is thus given as

$$y_t = \underbrace{\sqrt{\alpha_k}\mathbf{h}_k^{\text{H}}\left(\mathbf{w}x_d + \mathbf{s}_0\right)c_k}_{T_k\text{'s signal}} + \underbrace{\sum_{i\neq k}^{K}\sqrt{\alpha_i}\mathbf{h}_i^{\text{H}}\left(\mathbf{w}x_d + \mathbf{s}_0\right)c_i}_{\text{Muti-tag interference}} + z_u. \tag{7}$$

On the other hand, backscattered signals from tags reach the user and the BS. These signals can be sensed to extract state information of the tags [12]. The received signal at the BS is thus given as

$$\mathbf{y}_b = \underbrace{\sum_{k=1}^{K}\sqrt{\alpha_k}\mathbf{G}_k\mathbf{x}c_k}_{\text{Tags' reflections}} + \underbrace{\mathbf{H}_{\text{SI}}^{\text{H}}\mathbf{x}}_{\text{SI}} + \underbrace{\mathbf{z}_b}_{\text{AWGN}}, \tag{8}$$

where $\sqrt{\alpha_k}\mathbf{G}_k\mathbf{x}c_k$ is T_k's reflection and $\mathbf{z}_b \sim \mathcal{CN}(\mathbf{0}, \sigma^2\mathbf{I}_N)$ the AWGN at the BS. In (8), it is assumed that the BS applies clutter rejection techniques to mitigate the reflected clutter interference from the surrounding environment [14].

The FD BS cancels the SI at its receiver using perfect SI cancellation techniques [40], [41]. The post-processed signal is thus given as

$$\mathbf{y}'_b = \sum_{k=1}^{K} \sqrt{\alpha_k}\mathbf{G}_k\mathbf{x}c_k + \mathbf{z}_b. \tag{9}$$

The BS then applies the sensing combiner, $\mathbf{u}_k \in \mathbb{C}^{N\times 1}$ for $k \in \{1, \ldots, K\}$, to (9) to capture the desired reflected signal of T_k. The post-processed signal for obtaining T_k's sensing information is given as

$$\begin{aligned} y_{b,k} &= \mathbf{u}_k^{\mathrm{H}}\mathbf{y}'_b \\ &= \underbrace{\sqrt{\alpha_k}\mathbf{u}_k^{\mathrm{H}}\mathbf{G}_k\mathbf{x}c_k}_{T_k\text{'s desired reflection}} + \underbrace{\sum_{i\neq k}^{K}\sqrt{\alpha_i}\mathbf{u}_k^{\mathrm{H}}\mathbf{G}_i\mathbf{x}c_i}_{\text{Multi-tag interference reflections}} + \mathbf{u}_k^{\mathrm{H}}\mathbf{z}_b. \end{aligned} \tag{10}$$

Remark 1:
The following assumptions are standard and widely used: (i) For co-located transmit and receive arrays, the angles of T_k, i.e., θ_k, seen at the BS transceiver are the same in (8), a reasonable and common assumption [14], (ii) $\{\theta_k\}_{k=1}^K$ is assumed to be pre-estimated and known to the BS for beamformer/combiner design utilizing previous scannings [16], (iii) Because the BS and the user are linked via a controlled link, the user is aware of the sensing waveform in advance [48], and (iv) A dedicated channel estimating phase is used before FD transmission, ensuring CSI is available for beamforming design and SI cancellation at the BS, as well as SIC at the user/reader [49].

Remark 2:
Channel estimation and data transmission tasks occur in two separate time slots. In the initial slot, communication CSI, i.e., $\mathbf{f}$ and $\{\mathbf{h}_k\}_{k=1}^K$, can be estimated using emerging techniques [44], [50], [51]. These methods encompass pilot-based, blind, and semi-blind approaches, employing algorithms like least squares (LS), MMSE estimator, expectation maximization, and machine learning to achieve high-precision channel estimation [44], [50], [51]. However, as our study focuses on integrating sensing into BackCom, perfect CSI of communication channels is assumed [16], [52]. In addition, the instantaneous CSI, i.e., $\mathbf{f}$ and $\{\mathbf{h}_k\}_{k=1}^K$, is not required for the BS sensing operation since the sensing includes averaging over the received target/tag reflected signals. Similar to traditional ISAC systems, the long-term statistics of the echo channels are assumed to be known at the BS [16], [49], [52].

Current channel estimators are accurate with the cascaded channel $\mathbf{h}_k$, but do not separate the constituent channels, i.e., $\mathbf{g}_{f,k}$ and v_k [43], [44], [50]. However, using the structure of $\mathbf{g}_{f,k}$, i.e., the array response in (2), the parameter θ_k may be estimated using $\mathbf{h}_k$. Nevertheless, θ_k is not the only tags' state information extracted from a particular target echo signal. Other parameters, such as range, velocity, etc., must be estimated for tracking and environment mapping. Consequently, as proposed in this study, estimating the tags' state parameters necessitates a separate sensing framework. Conversely, the properties of T_k's reflected signal $\sqrt{\alpha_k}\mathbf{G}_k\mathbf{x}c_k$, such time of ToA, AoA, AoD, TDoA, RSS, and Doppler frequency/shifts, can be used to acquire tag's state information, such as range, angle, location, and velocity. Maximizing the echo signal strength for a particular tag while limiting tag interference at the BS, i.e., sensing SINR, improves tag detection probability and precise estimate of these targeted parameters. However, as the primary objective is integrating sensing into BackCom systems, the state parameter estimation is for future research.

III. Communication, Sensing, and EH Performance

The SINRs for sensing and communication tasks are the critical system parameters. Thus, these are derived next.

A. Communication Performance

The main communication SINRs are the user SINR and tags' SINRs.

1) User communication SINR

The user first decodes x_d, considering the tag signals as interference. From (6), the user communication SINR is thus obtained as

$$\Gamma_u^{\mathrm{Com}} = \frac{|\mathbf{f}^{\mathrm{H}}\mathbf{w}|^2}{\sum_{k=1}^{K}\alpha_k(|\mathbf{h}_k^{\mathrm{H}}\mathbf{w}|^2 + \mathbf{h}_k^{\mathrm{H}}\mathbf{S}\mathbf{h}_k) + \sigma^2}. \tag{11}$$

Here, while the user can cancel interference from the direct-link sensing signal, i.e., $\mathbf{f}^{\mathrm{H}}\mathbf{s}_0$, it cannot cancel interference from tag-sensing reflections because they consist of unknown tag data, i.e., c_k for $k \in \{1, \ldots, K\}$.

2) T_k's communication SINR

The user employs SIC to decode the backscatter data. Using (7), the communication SINR of T_k at the user is given as

$$\Gamma_{t,k}^{\mathrm{Com}} = \frac{\alpha_k\left(|\mathbf{h}_k^{\mathrm{H}}\mathbf{w}|^2 + \mathbf{h}_k^{\mathrm{H}}\mathbf{S}\mathbf{h}_k\right)}{\sum_{i\neq k}^{K}\alpha_i\left(|\mathbf{h}_i^{\mathrm{H}}\mathbf{w}|^2 + \mathbf{h}_i^{\mathrm{H}}\mathbf{S}\mathbf{h}_i\right) + \sigma^2}. \tag{12}$$

B. Sensing Performance

Sensing performance is typically evaluated by three measures: (a) transmit beampattern gain, (b) sensing SINR, or (c) sensing rate [47]. While (a) is simple, it may result in uncertainty in multi-target detection due to interference between the targets' reflected signals [16], [53]. Due to these limitations, (b) and (c) have recently been used widely (see Remark 3) [16], [53]. Specifically, sensing SINR is most

widely used in many ISAC studies [12], [16], [52], [53]. Consequently, this study will also employ it.

In multi-tag/target scenarios, the sensing SINR assists in improving the state parameter estimation for a particular tag/target [16], [52]. To sense the k-th tag, T_k, the BS applies the sensing combiner, $\mathbf{u}_k$, to the received signal (9). From (10), the sensing SINR associated with T_k is given by

$$\begin{aligned}\Upsilon_k^{\mathrm{Sen}} &= \frac{\alpha_k \mathbb{E}\left\{|\mathbf{u}_k^{\mathrm{H}}\mathbf{G}_k\mathbf{x}|^2\right\}}{\sum_{i\neq k}^{K}\alpha_i \mathbb{E}\left\{|\mathbf{u}_k^{\mathrm{H}}\mathbf{G}_i\mathbf{x}|^2\right\} + \mathbb{E}\left\{|\mathbf{u}_k^{\mathrm{H}}\mathbf{z}_b|^2\right\}} \\ &= \frac{\alpha_k \mathbf{u}_k^{\mathrm{H}}\mathbf{G}_k\mathbf{R}_x\mathbf{G}_k^{\mathrm{H}}\mathbf{u}_k}{\mathbf{u}_k^{\mathrm{H}}\left(\sum_{i\neq k}^{K}\alpha_i\mathbf{G}_i\mathbf{R}_x\mathbf{G}_i^{\mathrm{H}} + \sigma^2\mathbf{I}_N\right)\mathbf{u}_k}, \end{aligned} \tag{13}$$

where $\mathbf{R}_x \triangleq \mathbb{E}\{\mathbf{x}\mathbf{x}^{\mathrm{H}}\} = \mathbf{w}\mathbf{w}^{\mathrm{H}} + \mathbf{S}$ is the covariance matrix of the BS transmitted signal (4) [16]. Note that $\Upsilon_k^{\mathrm{Sen}}$ relies on the transmit signal covariance $\mathbf{R}_x$, sensing/echo channel gain $\mathbf{G}_k$, tag reflection coefficient α_k, and sensing combiner $\mathbf{u}_k$, which are constant for a given coherence interval. Hence, $\Upsilon_k^{\mathrm{Sen}}$ is constant.

Remark 3:
The sensing rate, measured in bps/Hz, implies the following [12], [16], [52], [53]:

1) It indicates how much environmental information can be extracted from the reflected signal of a target.
2) It helps to achieve efficient sensing waveform designs.

Hence, the quality of state parameter estimation is proportional to its sensing SINR of a target [16], [52], [53]. The sensing SINR and sensing rate are closely related. Thus, the goal is to increase the sensing rate for a specific target while minimizing interference from echo signals from other targets. Therefore, increasing the sensing rate helps state parameter estimation through echo signal processing [12], [16], [52], [53]. Additionally, the sensing SINR can be increased via transmit and receiver beampatterns (see Fig. 3 and Fig. 4). It thus aids in reducing interference between tags/targets.

Remark 4:
ISABC utilizes the reflections from the tags' antenna rather than their radar cross-section (RCS) or physical aperture reflections. This is because the primary objective is to extract the tags' state information, such as angle, velocity, and distance, rather than to measure the tags' structural properties (e.g., shape, orientation, or material composition) [14], [42]. The tag-antenna reflections, directly proportional to the reflection coefficients, α_k, provide sufficient information to achieve this goal [14], [42]. Specifically, they are sufficient for estimating spatial parameters like range, angle, and velocity. These parameters are critical for IoT applications like asset tracking, smart monitoring, and positioning [14], [42]. On the other hand, backscatter tags designed for IoT applications are typically compact and low-profile, optimized for minimal power usage [17], [18]. Consequently, their structural RCS is very small, contributing little to the reflected signal [54]. Therefore, in this initial work, we assume that reflections from the tags' structural RCS are negligible due to their weak and diffuse nature. Thus, the sensing SINR in (13) for extracting state information about the tag solely relies on the tags' antenna reflections.

C. Tags' EH

From Section E, the input power to the tag must exceed the activation threshold. The input power at T_k is given as

$$p_k^{\mathrm{in}} = |\mathbf{g}_{f,k}^{\mathrm{H}}\mathbf{w}|^2 + \mathbf{g}_{f,k}^{\mathrm{H}}\mathbf{S}\mathbf{g}_{f,k}. \tag{14}$$

IV. Problem Formulation

Our objective is to optimize the BS communication beamformer, $\mathbf{w}$, sensing signal (covariance) $\mathbf{S}$, sensing combiners, $\{\mathbf{u}_k\}_{k=1}^K$, alongside the tags' reflection coefficients, $\{\alpha_k\}_{k=1}^K$. The set of these optimization variables is denoted as $\mathcal{A} = \left\{\{\mathbf{u}_k\}_{k=1}^K, \{\alpha_k\}_{k=1}^K, \mathbf{w}, \mathbf{S} \succ 0\right\}$. The optimization criterion is minimizing the total BS transmit power. The resulting power efficiency can be exploited to enhance network capacity for additional tags and users. Thus, this optimization promotes large-scale connectivity. This approach benefits green IoT networks, reducing energy consumption, which extends network lifespans and efficiency [55].

Sensing performance metrics (e.g., detection probability or estimation accuracy) depend on the statistical properties of the waveform [56, Chapter 14]. The covariance matrix captures the power distribution and spatial properties needed to perform sensing tasks (e.g., angle estimation, range estimation) effectively [56]. Therefore, optimizing the sensing covariance matrix tends to achieve the desired sensing performance. Waveforms can be generated for a given optimum covariance matrix $\mathbf{S}$ to achieve the sensing beampattern and performance.

This goal is achieved by ensuring minimum communication SINR requirements (i.e., both primary and backscatter) at the user, the EH threshold of the tags, and the sensing SINR thresholds. The problem is thus formulated as follows:

$$\begin{aligned}
(\mathrm{P1}): \min_{\mathcal{A}} \quad & \|\mathbf{w}\|^2 + \mathrm{Tr}(\mathbf{S}), && \text{(15a)}\\
\text{s.t.} \quad & \Upsilon_k^{\mathrm{Sen}} \geq \Upsilon_{k,\mathrm{th}}^{\mathrm{Sen}}, \ \forall k, && \text{(15b)}\\
& \Gamma_u^{\mathrm{Com}} \geq \Gamma_{u,\mathrm{th}}^{\mathrm{Com}}, && \text{(15c)}\\
& \Gamma_{t,k}^{\mathrm{Com}} \geq \Gamma_{t,k,\mathrm{th}}^{\mathrm{Com}}, \ \forall k, && \text{(15d)}\\
& p_k^{\mathrm{in}} \geq \frac{\Phi^{-1}(p_b)}{1-\alpha_k}, \ \forall k, && \text{(15e)}\\
& \|\mathbf{u}_k\|^2 = 1, \ \forall k, && \text{(15f)}\\
& 0 < \alpha_k < 1, \ \forall k, && \text{(15g)}
\end{aligned}$$

where (15b) ensures the sensing SINR of T_k exceed the threshold $\Upsilon_{k,\mathrm{th}}^{\mathrm{Sen}}$. Specifically, this bound improves the echo signal quality for a particular tag, enabling estimation of the state parameters of the tag via echo signal processing [16], [49]. On the other hand, (15c) and (15d) set the communication SINR thresholds, i.e., $\Gamma_{u,\mathrm{th}}^{\mathrm{Com}}$ and $\Gamma_{t,k,\mathrm{th}}^{\mathrm{Com}}$, for the user to decode its own data and T_k's data, respectively.

These ensure the minimum quality of the rate for the user and tags. Constraint (15e) indicates the minimum incident power required at each tag for activation. Constraint (15g) specifies the natural bounds on the reflection coefficient of each tag.

Minimizing transmit power reduces energy consumption and costs, and extends network lifespan. Other metrics like latency, throughput, and reliability are of secondary importance. Thus, our formulation prioritizes communication/sensing SINR requirements while minimizing BS transmit power, aligning with the efficiency and robustness essential for green IoT deployments [55].

Nevertheless, the transmit power optimization approaches of ISABC and ISAC differ: ISABC uses backscatter tags, while ISAC relies on conventional targets. This introduces complexity and additional constraints to ISABC's optimization problem, (P1), specifically constraints (15d) and (15e) for tag data communication and energy harvesting, which are not present in ISAC. Consequently, ISAC has a significantly simpler optimization framework. However, ISABC enhances spectral efficiency through tag data communication.

Since the denominators of communication SINRs in (11) and (12) are similar (except for the k-th term), constraints (15c) and (15d) can be combined into a single constraint without changing the original problem (P1). In particular, we can rewrite (11) and (12) as

$$\alpha_k(|\mathbf{h}_k^{\mathrm{H}}\mathbf{w}|^2+\mathbf{h}_k^{\mathrm{H}}\mathbf{S}\mathbf{h}_k)\leq\frac{|\mathbf{f}^{\mathrm{H}}\mathbf{w}|^2}{\Gamma_{u,\mathrm{th}}^{\mathrm{Com}}}-\sum_{i\neq k}^{K}\alpha_i(|\mathbf{h}_i^{\mathrm{H}}\mathbf{w}|^2+\mathbf{h}_i^{\mathrm{H}}\mathbf{S}\mathbf{h}_i)+\sigma^2, \tag{16}$$

$$\alpha_k\left(|\mathbf{h}_k^{\mathrm{H}}\mathbf{w}|^2+\mathbf{h}_k^{\mathrm{H}}\mathbf{S}\mathbf{h}_k\right)\geq\Gamma_{t,k,\mathrm{th}}^{\mathrm{Com}}\times\left(\sum_{i\neq k}^{K}\alpha_i\left(|\mathbf{h}_i^{\mathrm{H}}\mathbf{w}|^2+\mathbf{h}_i^{\mathrm{H}}\mathbf{S}\mathbf{h}_i\right)+\sigma^2\right), \tag{17}$$

These two bounds in (16) and (17) can be integrated into the following constraint:

$$\left(\sum_{i\neq k}^{K}\alpha_i\left(|\mathbf{h}_i^{\mathrm{H}}\mathbf{w}|^2+\mathbf{h}_i^{\mathrm{H}}\mathbf{S}\mathbf{h}_i\right)+\sigma^2\right)\leq\frac{|\mathbf{f}^{\mathrm{H}}\mathbf{w}|^2}{\Gamma_{k,\mathrm{th}}^{\mathrm{Com}}}. \tag{18}$$

where $\Gamma_{k,\mathrm{th}}^{\mathrm{Com}}\triangleq\Gamma_{u,\mathrm{th}}^{\mathrm{Com}}(1+\Gamma_{t,k,\mathrm{th}}^{\mathrm{Com}})$. Thus, (P1) is equivalent to the following optimization problem:

$$(\mathrm{P2}):\ \min_{\mathcal{A}}\quad\|\mathbf{w}\|^2+\mathrm{Tr}(\mathbf{S}), \tag{19a}$$

$$\text{s.t}\quad(15\text{b}),\ (15\text{e})-(15\text{g}),(18). \tag{19b}$$

Our next step is to develop a new optimization algorithm to solve (19a).

V. Proposed Solution

Problem (19a) is non-convex due to its constraints set involving products of the optimization variables. To tackle this, the AO paradigm is utilized [25]. It is a divide-and-conquer strategy that divides an optimization problem into sub-problems that are easier to solve individually, then solved one at a time while keeping the other variables fixed. The process iterates until a stopping criterion is met. This approach works when directly optimizing all variables is challenging or computationally expensive [25]. Formally, to solve $\min_x f(x)$, where $x\in\mathbb{R}^s$ can be divided into $l>1$ blocks, i.e., $x=(x_1,x_2,\ldots,x_l)^{\mathrm{T}}$ with $x_l\in\mathbb{R}^{s_k}$ and $\sum_{k=1}^{l}s_k=s$, $f(x)$ is minimized over $x_k(k=1,\ldots,l)$, while holding $x_m|m\neq k$ at the prior values. The cycle repeats until convergence. AO achieves a locally optimal solution [25] (See Remark 5).

Thus, by following the AO paradigm, (19a) is divided into three sub-problems. Each optimizes (19a) for the associated variable(s) while keeping the other optimization variables fixed. The solution of each sub-problem then feeds into the next one. This block optimization process iterates until the objective function converges. In the first sub-problem, with constant communication beamformer $\mathbf{w}$, sensing signal covariance $\mathbf{S}$, and reflection coefficients $\{\alpha_k\}_{k=1}^K$, sensing combiners $\{\mathbf{u}_k\}_{k=1}^K$ are optimized using (15a). Subsequently, sensing combiners $\{\mathbf{u}_k\}_{k=1}^K$ and reflection coefficients $\{\alpha_k\}_{k=1}^K$ are fixed to optimize communication beamformer $\mathbf{w}$ and sensing signal covariance $\mathbf{S}$, navigating the non-convex constraints in (19a) via the SDR method [28], [29]. The last sub-problem, optimizing the reflection coefficients $\{\alpha_k\}_{k=1}^K$, is handled using a novel slack-optimization approach.

Although the original AO approach suggests that the same objective function be optimized over alternative blocks of variables [25], that is not the case here. In our case, the first and third sub-problems are independent of the original objective. These two, hence, are feasibility problems, where the primary goal is to find a feasible solution that satisfies a set of constraints. Feasibility problems focus solely on finding a point that meets the specified constraints, without necessarily optimizing any objective. Nonetheless, these are transformed into optimization problems with explicit objectives to achieve more efficient solutions without compromising the original problem. Consequently, our approach may yield a considerably efficient solution [29].

A. Sub-Problem 1: Optimization Over $\mathbf{u}_k$

For given $\{\mathbf{w},\mathbf{S},\{\alpha_k\}_{k=1}^K\}$, problem (P2) becomes a feasibility problem for sensing combiners, $\{\mathbf{u}_k\}_{k=1}^K$. This is because the BS transmit power minimization, i.e., the goal of (19a), is independent of $\mathbf{u}_k$. Any feasible $\mathbf{u}_k$ that satisfies the constraints (15b) and (15f) can thus be a solution.

Although $\mathbf{u}_k$ may not directly reduce BS transmit power, the sensing SINR at the BS for each tag depends on an optimal choice of $\mathbf{u}_k$. Thus, maximizing the sensing SINR for each tag serves a dual purpose: it ensures that sensing performance criteria are met and indirectly aids in transmit power reduction. Ensuring high SINR for tag signals can reduce the need for increased transmit power to counter poor reception, aligning with our power minimization strategy.

Optimizing $\mathbf{u}_k$ to maximize sensing SINR supports power minimization in the subsequent AO steps [26], [27].

Utilizing the unique structure of the sensing SINR for each tag (13) transforms this sub-problem into a generalized Rayleigh quotient optimization problem, which has a direct closed-form solution [26], [27]. Consequently, the following optimization problem arises:

$$\text{(P3)}: \max_{\mathbf{u}_k} \quad \frac{\alpha_k \mathbf{u}_k^{\mathrm{H}} \mathbf{G}_k \mathbf{R}_x \mathbf{G}_k^{\mathrm{H}} \mathbf{u}_k}{\mathbf{u}_k^{\mathrm{H}} \left(\sum_{i \neq k}^{K} \alpha_i \mathbf{G}_i \mathbf{R}_x \mathbf{G}_i^{\mathrm{H}} + \sigma_k^2 \mathbf{I}_N \right) \mathbf{u}_k}, \tag{20a}$$

$$\text{s.t} \quad \|\mathbf{u}_k\|^2 = 1, \ \forall k. \tag{20b}$$

The objective function in (20a) can be restated as the following optimization problem:

$$\text{(P4)}: \max_{\mathbf{u}_k} \frac{\mathbf{u}_k^{\mathrm{H}} \tilde{\mathbf{g}}_k \tilde{\mathbf{g}}_k^{\mathrm{H}} \mathbf{u}_k}{\mathbf{u}_k^{\mathrm{H}} \mathbf{Q} \mathbf{u}_k}, \quad \text{s.t} \quad \|\mathbf{u}_k\|^2 = 1, \ \forall k, \tag{21a}$$

where $\tilde{\mathbf{g}}_k = \sqrt{\alpha_k} \mathbf{G}_k (\mathbf{w} + \mathbf{s})$ and $\mathbf{Q} = \sum_{i \neq k}^{K} \alpha_i \mathbf{G}_i \mathbf{R}_x \mathbf{G}_i^{\mathrm{H}} + \sigma_k^2 \mathbf{I}_N$. Problem (P4) in (21a) is a generalized Rayleigh ratio quotient problem [26], [27]. When $\mathbf{w}$, $\mathbf{S}$, and $\{\alpha_k\}_{k=1}^K$ are fixed, the optimal sensing combiner is thus given by

$$\mathbf{u}_k^* = \frac{\mathbf{Q}^{-1} \tilde{\mathbf{g}}_k}{\|\mathbf{Q}^{-1} \tilde{\mathbf{g}}_k\|}, \ \forall k, \tag{22}$$

which is an MMSE filter [26], [27].

B. Sub-Problem 2: Optimization Over $\mathbf{w}$ and $\mathbf{S}$

For given $\{\{\mathbf{u}_k\}_{k=1}^K, \{\alpha_k\}_{k=1}^K\}$, problem (P2) can be reformulated as the following equivalent problem:

$$\text{(P5)}: \min_{\mathbf{w}, \mathbf{S}} \quad \|\mathbf{w}\|^2 + \mathrm{Tr}(\mathbf{S}), \tag{23a}$$

$$\text{s.t} \quad (18), \ (15b), \ (15e). \tag{23b}$$

This also yields the sensing signal $\mathbf{s}_0$, the eigenvector of the maximum eigenvalue of $\mathbf{S}$ [47]. Problem (23a) is effectively solved by the SDR method [28], [29]. To use it, consider matrix $\mathbf{W} = \mathbf{w}\mathbf{w}^{\mathrm{H}}$. Clearly, $\mathbf{W}$ is semidefinite and has $\mathrm{Rank}(\mathbf{W}) = 1$. Thus, the SDR approach reformulates problem (23a) as (24), where the rank-one constraint is relaxed.

Note that the rank-relaxed (24) represents a conventional semi-definite programming (SDP) problem [57], which can be solved using the CVX tool [57], [58]. Let a solution to (23a) be $\mathbf{W}^* = \mathbf{U}\mathbf{\Sigma}\mathbf{U}^{\mathrm{H}}$ where $\mathbf{U}$ is a unitary matrix and $\mathbf{\Sigma} = \mathrm{diag}(\lambda_1, \ldots, \lambda_M)$ is a diagonal matrix, both sized $M \times M$. If it turns out to be rank one, $\mathbf{W}^*$ itself is the optimal communication beamformer. Otherwise, a rank-one solution must be extracted from it via Gaussian randomization [29]. Specifically, a randomized solution to (23a) is constructed from $\mathbf{W}^*$, which is given by $\bar{\mathbf{W}} = \mathbf{U}\mathbf{\Sigma}^{1/2}\mathbf{r}$, with $\mathbf{r} \in \mathcal{CN}(0, \mathbf{I}_M)$. This is repeated for 10^5 times, and the best solution is selected. These numerous random realizations of $\mathbf{r}$ with the SDR technique ensure a $\frac{\pi}{4}$-approximation to the optimal value of (23a) [28], [29].

C. Sub-Problem 3: Optimization Over α_k

This one optimizes each tag's reflection coefficient (α_k). By isolating the variables and constraints relevant to this sub-problem, the original optimization problem (15a) can be recast into a feasibility problem as follows:

$$\text{(P7)}: \text{find} \quad \alpha_k \tag{25a}$$

$$\text{s.t} \quad (15b) - (15e), \ (15g), \tag{25b}$$

where any α_k that satisfies (P7) is considered a feasible solution. However, the feasible solution yielded from (P7) does not guarantee that the constraints are satisfied with equality [29]. Hence, to achieve a better solution, it can be transformed into an optimization problem with an explicit objective to obtain generally more efficient reflection coefficients to reduce the transmit power [29]. The rationale is that for the communication beamformer and sensing signal optimization problem, i.e., (P6) (24), all SINRs and EH constraints are active at the optimal solution; thus, optimizing the reflection coefficient to force the tag communication and sensing SINRs and EH to be greater than the targeted values in (P8) directly leads to a reduction in transmit power in (P6) [29]. Following the slack variable technique in [29], [30], two new slack variables, t_1 and t_2, which represent the "sensing SINR residual" and "EH residual," are introduced to optimize the sensing SINR and EH margins further while satisfying constraint (25b). The following sub-problem needs to be solved:

$$\text{(P8)}: \min_{\alpha_k, t_1, t_2} \quad \lambda_1 t_1 + \lambda_2 t_2 \tag{26a}$$

$$\text{s.t} \quad \alpha_k \mathbf{u}_k^{\mathrm{H}} \mathbf{G}_k \mathbf{R}_x \mathbf{G}_k^{\mathrm{H}} \mathbf{u}_k \geq \tag{26b}$$

$$\Upsilon_{k,\mathrm{th}}^{\mathrm{Sen}} \mathbf{u}_k^{\mathrm{H}} \left(\sum_{i \neq k}^{K} \alpha_i \mathbf{G}_i \mathbf{R}_x \mathbf{G}_i^{\mathrm{H}} + \sigma_k^2 \mathbf{I}_N \right) \mathbf{u}_k + t_1, \forall k,$$

$$\frac{|\mathbf{f}^{\mathrm{H}} \mathbf{w}|^2}{\Gamma_{k,\mathrm{th}}^{\mathrm{Com}}} - \sum_{i \neq k}^{K} \alpha_i \left(|\mathbf{h}_i^{\mathrm{H}} \mathbf{w}|^2 + \mathbf{h}_i^{\mathrm{H}} \mathbf{S} \mathbf{h}_i \right) \geq \sigma^2, \forall k, \tag{26c}$$

$$(1 - \alpha_k) p_k^{\mathrm{in}} \geq \Phi^{-1}(p_b) + t_2, \forall k, \tag{26d}$$

$$(15g), \tag{26e}$$

where λ_1 and λ_2 are positive constants. Problem (26a) is convex and thus can be efficiently solved by solvers such as CVX [58]. Although (25a) and (26a) share the same feasible set, the introduction of slack variables in (26a) converts strict constraints into adjustable ones with a definable margin. This facilitates the convergence process by setting a more tangible minimization goal and aligns well with the convergence strategies of iterative solvers like CVX due to the explicit objective guiding the solution path [29].

Our algorithm to solve (15a) is presented in Algorithm 1. It starts by initializing $\{\{\alpha_k\}_{k=1}^K, \mathbf{w}, \mathbf{S}\}$ to random feasible values and, in every iteration, refines the values of $\left\{\{\mathbf{u}_k\}_{k=1}^K, \{\alpha_k\}_{k=1}^K, \mathbf{w}, \mathbf{S}\right\}$ until the normalized improvement of the objective function F, i.e., total transmit power, is smaller than convergence tolerance $\epsilon = 1 \times 10^{-3}$.

$$
\begin{aligned}
(\text{P6}): \ & \underset{\mathbf{W},\mathbf{S}}{\text{minimize}} \ \text{Tr}(\mathbf{W}) + \text{Tr}(\mathbf{S}) \\
\text{s.t} \ & \Upsilon_{k,\text{th}}^{\text{Sen}} \mathbf{u}_k^{\text{H}} \left(\sum_{i \neq k}^{K} \alpha_i \left(\text{Tr}(\mathbf{G}_i^{\text{H}} \mathbf{G}_i \mathbf{W}) + \text{Tr}(\mathbf{G}_i^{\text{H}} \mathbf{G}_i \mathbf{S}) \right) + \sigma_k^2 \mathbf{I}_N \right) \mathbf{u}_k - \alpha_k \mathbf{u}_k^{\text{H}} \left(\text{Tr}(\mathbf{G}_i^{\text{H}} \mathbf{G}_i \mathbf{W}) + \text{Tr}(\mathbf{G}_i^{\text{H}} \mathbf{G}_i \mathbf{S}) \right) \mathbf{u}_k \leq 0, \forall k, \\
& \frac{\text{Tr}(\mathbf{f}\mathbf{f}^{\text{H}} \mathbf{W})}{\Gamma_{k,\text{th}}^{\text{Com}}} - \sum_{i \neq k}^{K} \alpha_i \left(\text{Tr}(\mathbf{h}_i \mathbf{h}_i^{\text{H}} \mathbf{W}) + \text{Tr}(\mathbf{h}_i \mathbf{h}_i^{\text{H}} \mathbf{S}) \right) \geq \sigma^2, \forall k, \\
& P_{\text{th}} - (1 - \alpha_k)(\text{Tr}(\mathbf{g}_{f,k} \mathbf{g}_{f,k}^{\text{H}} \mathbf{W}) + \text{Tr}(\mathbf{g}_{f,k}^{\text{H}} \mathbf{g}_{f,k} \mathbf{S})) \leq 0, \forall k. \qquad (24)
\end{aligned}
$$

Algorithm 1 : Overall AO Algorithm

1: **Input**: K, $\mathbf{f}$, $\{\mathbf{h}_k\}_{k=1}^K$, $\{\mathbf{G}_k\}_{k=1}^K$.
2: **Parameters**: Set $t = 0$, $\epsilon > 0$, $F^{(0)} = 0$.
3: **Initial feasible solution**: $\{\alpha_k^{(0)}\}_{k=1}^K, \mathbf{w}^{(0)}, \mathbf{S}^{(0)}$.
4: **while** $\frac{F^{(t+1)} - F^{(t)}}{F^{(t+1)}} \geq \epsilon$ **do**
5: Solve (P3) to obtain the sensing combiner, $\mathbf{u}_k^{(t+1)}$.
6: Solve (P5) to obtain communication beamformer $\mathbf{w}^{(t+1)}$ by recovering a rank-one solution via Gaussian randomization and sensing signal $\mathbf{s}_0^{(t+1)}$ using the covariance $\mathbf{S}^{(t+1)}$.
7: Solve (P8) to obtain the reflection coefficients, $\alpha_k^{(t+1)}$.
8: Calculate $F^{(t+1)}$.
9: Set $t \leftarrow t + 1$;
10: **end while**
11: **Output**: Optimal solutions $\mathcal{A}^*$.

Remark 5:
The convergence of the AO algorithm to a local minimum or stationary point is generally guaranteed for a wide range of problems, provided that certain conditions are met [25]. These conditions may include the objective function being lower-bounded and having certain smoothness properties. Specifically, as long as the individual sub-problems converge, the overall optimization also converges [25]. By exploiting that insight, the SDR and slack-optimization methods are used to solve $\{\mathbf{w}, \mathbf{s}_0\}$ and $\{\alpha_k\}_{k=1}^K$, respectively, whereas $\{\mathbf{u}_k\}_{k=1}^K$ is obtained as a closed-form solution applying the Rayleigh ratio quotient approach. SDR and slack-optimization are well-developed approaches with provable convergence [28], [29], ensuring the convergence of the proposed AO algorithm. Our simulations also validate this claim (Fig. 2).

Theorem 1:
Algorithm 1 iterations yield a non-increasing sequence of objective values with guaranteed convergence.

Proof:
Please see Appendix A. ■

D. Computational Complexity of the Proposed Algorithm

This is analyzed for the three sub-problems.

1) Optimization over $\mathbf{u}_k$

During this phase, the optimal sensing combiners are obtained using the Rayleigh quotient. Computing the inverse of the matrix $\mathbf{Q}$ requires $\mathcal{O}(N^3)$. Additionally, the MMSE filter for the K tags (as shown in (22)) adds complexity of $\mathcal{O}(KN^2)$. Therefore, the total complexity for this section is $\mathcal{O}(KN^2 + N^3)$.

2) Optimization over $\mathbf{w}$ and $\mathbf{S}$

Note that the interior-point method can solve sub-problems based on the SDP. According to [59, Th. 3.12], the order of complexity for a SDP problem with m SDP constraints which includes a $n \times n$ positive semi-definite (PSD) matrix is given by $\mathcal{O}\left(\sqrt{n} \log\left(\frac{1}{\epsilon}\right)(mn^3 + m^2n^2 + m^3)\right)$, where $\epsilon > 0$ is the solution accuracy. For problem (23a), with $n = M$ and $m = 3K+2$, the approximate computational complexity for solving (23a) can be written as $\mathcal{O}\left(KM^3\sqrt{M}\log\left(\frac{1}{\epsilon}\right)\right)$.

3) Optimization over α_k

Utilizing CVX, the optimization leverages the difference of convex functions (DC) and interior point methods. The iterations required for convergence can be expressed as $\frac{\left(\log(C)/t^0\delta\right)}{\log\epsilon}$. Here, C denotes the overall number of constraints. The term t^0 signifies the initial approximation for the interior point method's accuracy. The stopping criterion is $0 < \delta \ll 1$ [57].

4) Algorithm 1

The computational complexity of each iteration of Algorithm 1 is asymptotically equal to $\mathcal{O}\left(T\left(KN^2 + N^3 + KM^3\sqrt{M}\log\left(\frac{1}{\epsilon}\right) + \frac{\left(\log(C)/t^0\delta\right)}{\log\epsilon}\right)\right)$, where T is the required number of iterations for the outer algorithm to converge. Despite its higher-order polynomial time complexity, the proposed algorithm demonstrates commendable real-world performance for datasets up

TABLE 3: Simulation parameters.

Parameter	Value	Parameter	Value
B	10 MHz	$\Gamma^{\mathrm{Com}}_{t,k,\mathrm{th}}$	1 bps/Hz
N_f	10 dB	p_b	-20 dBm
$M = N$	8	M_{NL}	20×10^{-3} W
K	3	a_{NL}	6400
$\Upsilon^{\mathrm{Sen}}_{k,\mathrm{th}}$	1 bps/Hz	b_{NL}	0.003
$\Gamma^{\mathrm{Com}}_{u,\mathrm{th}}$	1 bps/Hz	$\{\lambda_1, \lambda_2\}$	1

to a particular size, predominantly when N and M are maintained below a defined threshold.

VI. Simulation Results

Simulation results are next presented to assess the performance of the proposed ISABC network and the AO algorithm.

A. Simulation Setup and Parameters

The 3GPP urban micro (UMi) model is adopted to model the path loss $\{\zeta_a, \zeta_b\}$ with $f_c = 3$ GHz operating frequency [60, Table B.1.2.1]. The considered AmBC leverages the existing RF signals for data transmission. The carrier frequency choice is thus compatible with existing standards and aligns with the future-forward vision of AmBC systems for 5G/6G spectrum utilization trends. The AWGN variance, σ^2, is modeled as $\sigma^2 = 10\log_{10}(N_0 B N_f)$ dBm, where $N_0 = -174$ dBm/Hz, B is the bandwidth, and N_f is the noise figure. Unless otherwise specified, Table 3 summarizes the simulation parameters. Each simulation point is averaged over 10^3 iterations.

For a typical smart home use case, the BS and the mobile reader are placed at $\{0, 0\}$ and $\{12, 0\}$, respectively, while the tags are randomly distributed within a circle centered at $\{6, -4\}$ with a radius of 3 m [61], [62].

B. Benchmark Schemes

The proposed ISABC system with passive backscatter tags is denoted by 'ISABC-P.' For comparative evaluation purposes, the following benchmarks are considered:

1) Convectional ISAC

The first benchmark 'ISAC' is conventional ISAC with a FD BS [16], [63]. This model does not include passive tags but conventional radar targets that only reflect incident signals and do not send data to the user. However, the sensing signal $\mathbf{s}_0$ does interfere with the detection process at the user. It is assumed to be perfectly canceled at the user and the BS [63]. However, the reflected signals by the targets cause interference for the user.

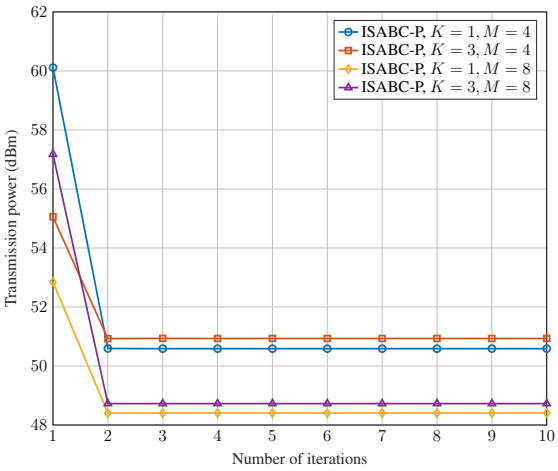

FIGURE 2: Convergence rate.

2) Conventional BackCom

This benchmark ('BackCom') comprises one user and multiple tags. The BS does not perform sensing; hence, the transmit signal becomes $\mathbf{x} = \mathbf{w}x_d$. The tags perform EH and backscatter $\mathbf{x}$ to send data. Thus, this benchmark helps to evaluate the cost of incorporating sensing functions on BackCom communication performance.

3) Communication-only scheme

This benchmark (legend 'Com-only') assesses the system's core communication capacity by focusing solely on a single-user scenario. It establishes a baseline performance metric by isolating communication from sensing and backscattering. Deviations from this metric reveal the impact of added sensing and backscattering.

4) Sensing-only scheme

This benchmark (legend 'Sensing-only') focuses on a sensing-centric system considering EH, excluding primary communication and BackCom. It helps establish a baseline for assessing trade-offs in integrated systems and highlights the system's raw sensing performance, particularly in cases prioritizing sensing over sporadic or secondary communications.

5) ISABC with active tags

Benchmark 'ISABC-A' evaluates the performance of the ISABC system with active tags (battery-powered), eliminating the need for EH requirements at the tags and thus reducing the BS transmit power. This benchmark thus establishes a baseline to gauge the cost to ISABC of ensuring EH at the tags.

Our Algorithm 1 accommodates all these benchmarks as special cases. Three more benchmarks are explored based on the tag's reflection coefficient and BS sensing combiners.

6) *Random reflection coefficients:* Tags might reflect signals without a set pattern, leading to random reflection coefficients. Such randomness can arise from environmental changes, tag characteristics, or varied communication protocols [64]. In contrast, optimizing reflection coefficients helps select the proper impedances, enhancing rates and ranges. Yet, this optimization requires more computational resources from the reader. For certain cost-sensitive applications, such an approach might not be economical. Thus, this baseline seeks to gauge the tradeoff between optimizing the tag reflection coefficients and not optimizing.

The next two benchmarks are motivated by the following considerations. Algorithm 1 aims to boost the sensing SINR, focusing especially on sub-problems (P4). The outcome of this strategy is the MMSE filter, as shown in (22). This algorithm iteratively refines the MMSE filter, drawing insights from its other two sub-problems. One might consider omitting a sub-problem to streamline this process by opting for simpler solutions for each $\mathbf{u}_k$ for $k \in \{1, \ldots, K\}$. Many receivers have leaned towards match filter (MF) and zero-forcing (ZF) combiners due to their simplicity [65]. However, MF struggles with multi-tag interference, while ZF is best suited for high SNR regions because of its sensitivity to noise. Thus, MF and ZF sensing combiners are developed next.

7) *MF sensing combiner:* $\mathbf{u}_{\text{MF}} = \mathbf{H}_b$, where this leverages the CSI to amplify the received signal's strength. Though advantageous in several scenarios, the MF combiner's inability to eliminate multi-tag interference is a limitation.
8) *ZF sensing combiner:* $\mathbf{u}_{\text{ZF}} = \mathbf{H}_b \left(\mathbf{H}_b^{\text{H}}\ qH_b\right)^{-1}$, which strives to obliterate interference at non-intended receivers by distinctively utilizing the CSI. It effectively manages interference, but its susceptibility to noise, especially in low-SNR environments, is challenging.

Elaborating further, $\mathbf{H}_b \in \mathbb{C}^{N \times K}$ symbolizes the backward channel matrix. Within this matrix, each k-th column's vector is articulated as $\mathbf{g}_{b,k}$ for $k \in \{1, \ldots, K\}$. Interestingly, these combiners rely solely on CSI, in stark contrast to the MMSE filter (22), which is influenced by tag reflection coefficients and the precoder. Utilizing the aforementioned combiners might lead to inferior performance concerning transmit power. Nevertheless, this paves the way for simplifying the three-stage AO approach into a more concise two-stage algorithm, which inherently means a faster algorithmic execution.

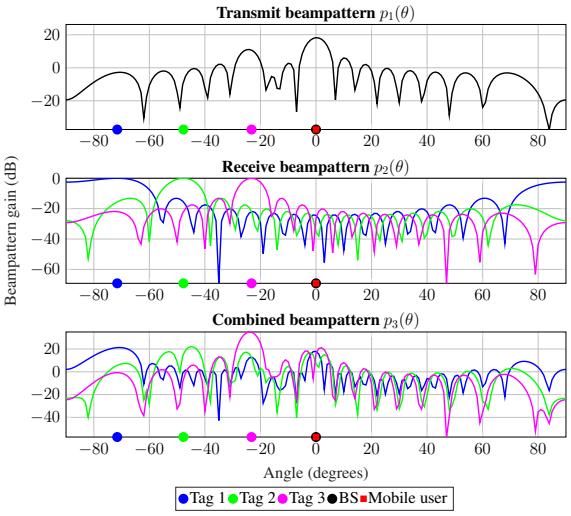

FIGURE 3: Beampattern of the radar functionality of Algorithm 1.

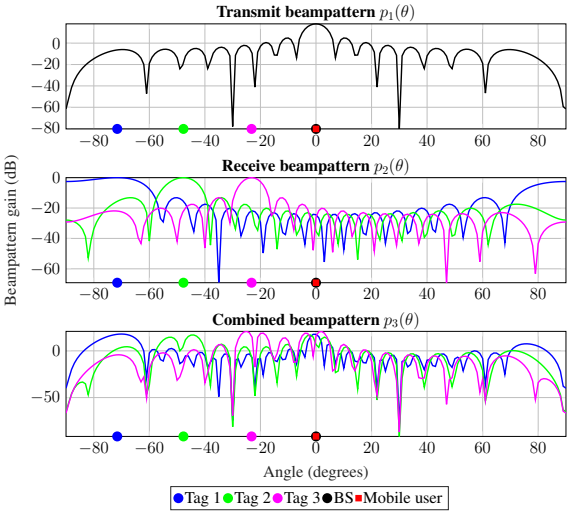

FIGURE 4: Beampattern of communication functionality, i.e., without dedicated $\mathbf{s}_0$.

C. Convergence Rate of Algorithm 1

This outputs the optimal BS sensing combiners, $\{\mathbf{u}_k\}_{k=1}^K$, BS communication beamformer and sensing signal, $\mathbf{w}$ and $\mathbf{s}_0$, respectively, and the tag reflection coefficients, $\{\alpha_k\}_{k=1}^K$, for a given ISABC system setup within several iterations. The BS power converges in several iterations. To measure the convergence rate, Fig. 2 plots the BS transmit power as a function of the number of iterations. About three iterations appear sufficient, regardless of M or K. In sum, Algorithm 1 achieves rapid convergence with any system configuration.

D. Beampattern Gains

Modern radar functionality has evolved to harness the power of beamforming, i.e., directly transmit and receive beams in specific directions. Algorithm 1 serves this function, guiding

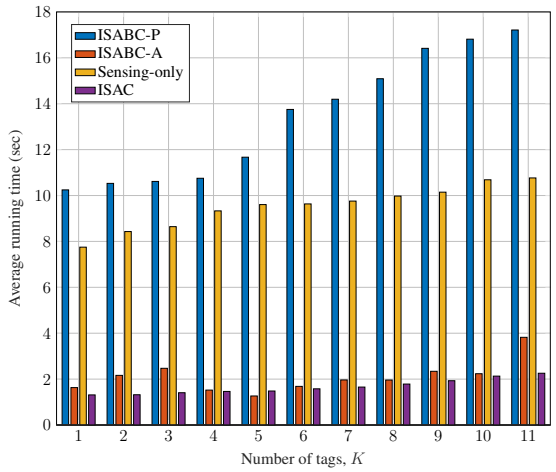

FIGURE 5: The running time versus the number of tags, K.

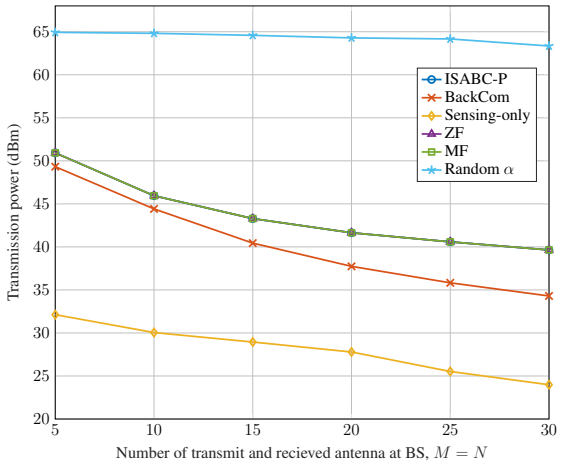

(a)

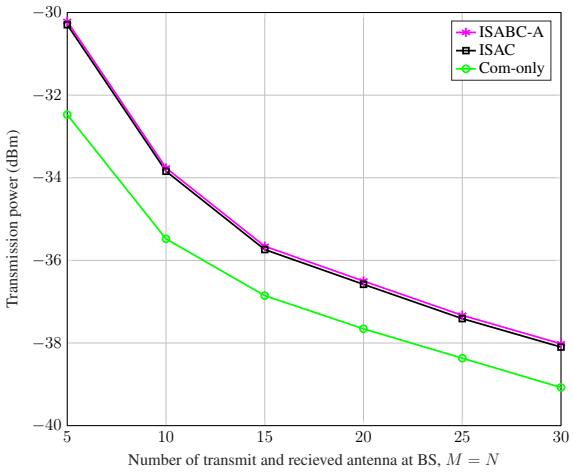

(b)

FIGURE 6: Transmit power versus the number of antennas at the BS, $M = N$.

the formation and steering of these beams. Beamforming in radar systems converges signals from an array of antennas, crafting a directed "beam" or "lobe" [16], [66]. Intriguingly, this beam can be electronically steered while the antennas remain stationary. This electronic steering capability amplifies signal quality, boosts backscatter tag detection, and significantly minimizes potential interference [16], [66].

The transmit signal, representing the outward-projected energy, is critical in efficiently illuminating the radar's targets. Meanwhile, the sensing combiner, normalized as $\|\mathbf{u}_k^*\| = 1$, is optimized for clear reception, capturing the echoes or reflections off the backscatter tags. Three pivotal beampatterns arise from these components:

$$p_1(\theta) = \left|\mathbf{b}^{\mathrm{H}}(\theta_k)\mathbf{x}^*\right|^2, \tag{27a}$$

$$p_2(\theta) = \left|(\mathbf{u}_k^*)^{\mathrm{H}}\mathbf{b}(\theta_k)\right|^2, \tag{27b}$$

$$p_3(\theta) = \left|(\mathbf{u}_k^*)^{\mathrm{H}}\mathbf{b}(\theta_k)\mathbf{b}^{\mathrm{H}}(\theta_k)\mathbf{x}^*\right|^2. \tag{27c}$$

First, (27a) illustrates how the transmitted energy disperses as a function of angle θ. Second, (27b) encapsulates the sensitivity of the radar system across different angles during the reception of reflected energy. Finally, (27c) offers a combined representation, integrating the effects of transmission and subsequent reflection processing. Fig. 3 and Fig. 4 help to gauge the effectiveness of beamforming algorithms.

E. Running Time Versus Number of Tags

Fig. 5 shows the correlation between the execution time and the number of tags, K. These data are from Matlab simulations for an Intel® Xeon® CPU, clocking at 3.5 GHz. Fig. 5 depicts a directly proportional trend between K and the running time for all schemes. This is due to an increase in computation demands as K increases. This tendency emphasizes the complicated challenges of dealing with a larger number of tags, underlining the necessity of efficient algorithms.

Compared to the ISABC-P and sensing-only schemes, the conventional ISAC approach achieves significantly lower runtime. This is because the algorithm for ISAC does not account for EH constraints, as the passive targets, in this case, do not require EH. In contrast, the proposed ISABC-P scheme has the highest runtime, driven by the need to meet the EH requirements of passive tags. Meanwhile, the ISABC-A system bypasses EH entirely using battery-powered tags, reducing runtime. For instance, with six tags, ISABC-A requires only 6.76 % more execution time than ISAC. Therefore, depending on the application scenario, one can opt for active tags instead of passive tags, balancing cost and tag architecture considerations.

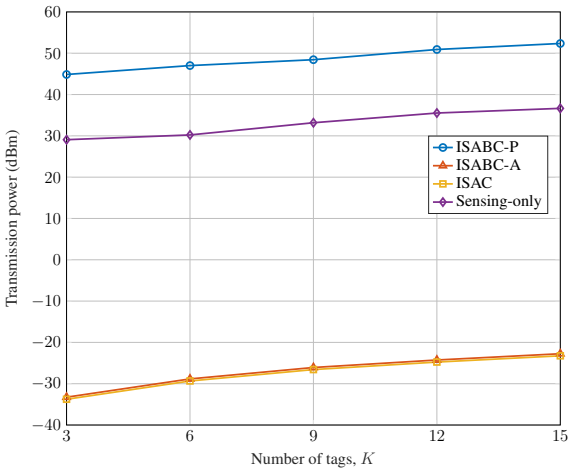

FIGURE 7: Transmit power versus the number of tags, K.

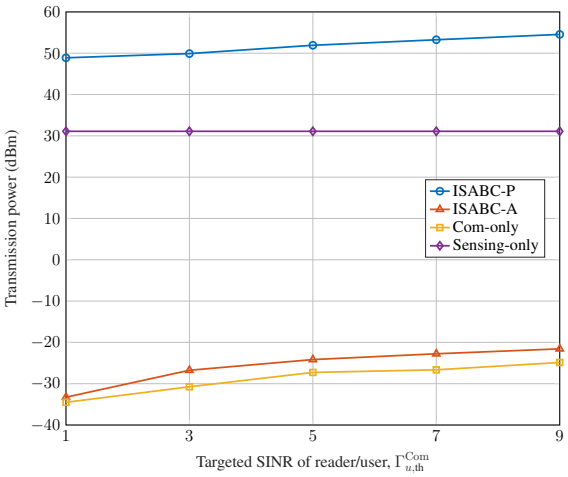

FIGURE 8: Transmit power versus the targeted communication SINR of the reader/user.

F. Transmit Power Versus Number of Antenna at the BS

The BS transmit power depends on the number of BS transmitter (M) and receiver (N) antennas, where $M = N$. In Fig. 6, a clear and consistent trend emerges across all schemes: increasing M decreases the transmit power. Thus, the two benefits of exploiting spatial diversity are increased communication rates and reduced power consumption.

Fig. 6a and Fig. 6b show the BS transmit power requirement as a function of M. As per Fig. 6a, the random-α benchmark is the most inefficient regarding energy use. The sensing-only approach requires less transmit power than ISABC-P, as it eliminates the communication performance. Furthermore, suboptimal MRT- and ZF-based beamformers closely align with our proposed schemes but need CSI. Importantly, ISABC-P allows for sensing with low-cost tags, an essential feature for IoT networks, with only a slight increase in transmit power. For instance, a $3.4\,\%$ increase in transmit power with $M = N = 10$ results in a $75\,\%$ sum rate gain, i.e., user rate + tags' rate + sensing rate.

Fig. 6b reveals that ISAC and communication-only methods require less BS transmit power than the proposed ISABC-P. The latter needs more BS power to deliver sufficient power at the tags for EH. Of course, this is the cost of using entirely passive tags. Nevertheless, utilizing active tags, as in ISABC-A, can prevent the need for this additional power at the BS. For instance, with $M = N = 10$, ISABC-A only requires a $0.24\,\%$ increase in transmit power to provide a $75\,\%$ sum rate gain over conventional ISAC. However, active tags with complex tag designs are more expensive than passive tags, and the type of tag used may vary depending on the application [6], [7].

G. Transmit Power Versus Number of Tags

Fig. 7 illustrates the interplay between the number of tags (K) and the BS transmit power. It suggests a linear correlation between these two variables across all schemes. Unlike conventional ISAC, ISABC-P and sensing-only approaches require more BS power to ensure sufficient EH for the tags (constraint (15e)). However, as previously stated, utilizing active tags (ISABC-A) can minimize the increased power demand compared to standard ISAC systems. This comes at a higher tag cost [6], [7].

H. Transmit Power Versus Communication SINR targets

Fig. 8 examines the relationship between the BS transmit power and the targeted user SINR, $\Gamma_{u,\text{th}}^{\text{Com}}$. Communication-only, sensing-only, and ISABC-P/A schemes are also plotted for a comprehensive comparison.

In the communication-only scheme, the BS requires minimal power to meet the user's rate demand. In the sensing-only approach with passive tags, the BS maintains steady power for energy harvesting (EH) and sensing without communication. The proposed ISABC-P requires higher BS transmit power to support primary communication and sensing services essential for future ambient-powered IoT networks. Alternatively, active tags (ISABC-A) can eliminate this higher power requirement at the BS, though they are more costly and complex to maintain than passive tags [6], [7].

I. Communication Impairments

CSI and SI cancellation errors degrade the performance and reliability of wireless links. CSI errors affect signal reception and beamforming. Moreover, SI cancellation errors occur when SI is not eliminated, hindering incoming signal reception. Both errors critically impair communication dynamics [67].

The impact of these errors on Algorithm 1 is explored in Fig. 9. The relation $\hat{x} = x + e$ models the channel estimation process [67], [68]. Here, the true channel is denoted by $x \in \{f_m, v_k\}$, for $m \in \{1, \ldots, M\}$ and $k \in \{1, \ldots, K\}$,

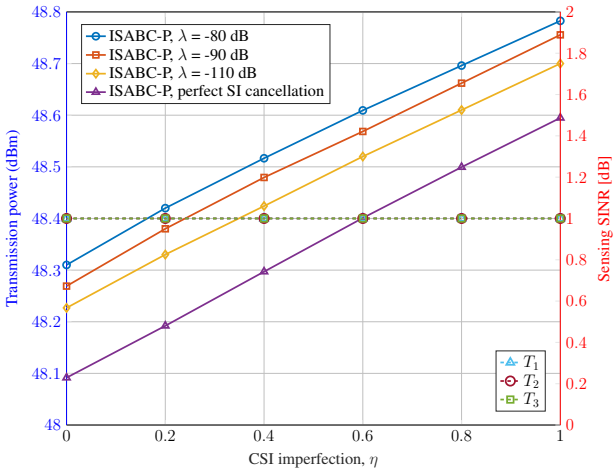

FIGURE 9: Transmit power (left y-axis) and sensing SINR (right y-axis) as functions of communication CSI imperfection η, for various residual SIC values.

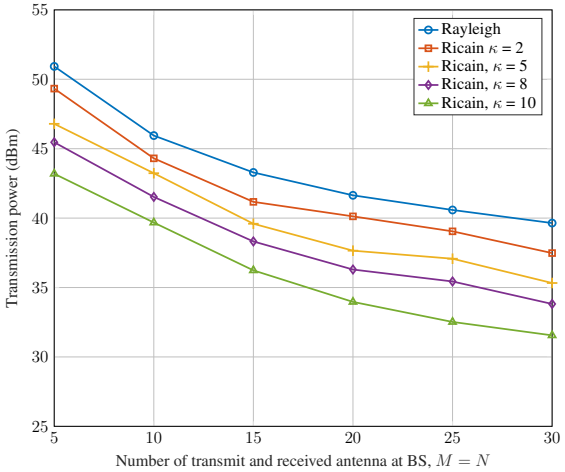

FIGURE 10: Transmit power for different fading channels.

and the term e denotes estimation noise distributed as $e \sim \mathcal{N}(0, \sigma_e^2)$. A critical parameter is the error variance, which is modeled as $\sigma_e^2 = \eta|x|^2$, where $|x|$ is the magnitude of the true channel value and $0 \leq \eta \leq 1$ accounts for the channel estimation quality [67], [68]. Here, η is a measure of CSI error magnitude. Fig. 9 displays the correlation between η and the transmit power. A clear positive correlation exists, i.e., increasing CSI errors increases transmit power requirements.

To model imperfect SI cancellation, the residual SI term, given by $\lambda|\mathbf{f}^{\mathrm{H}}\mathbf{w}|^2$, is included in the SINR of T_k. The variable $\lambda \in [0, 1]$ indicates the degree of imperfection in SI cancellation. Further experiments shed light on the transmission power in scenarios with varied values of residual SI, especially under the influence of distinct CSI errors. The transmit power is sacrificed as λ increases.

Fig. 9 also shows the sensing SINR (i.e., right y-axis) as a function of η. It reveals that regardless of the degree of imperfection, our algorithm can meet the minimum sensing SINR target for all tags. It thus compensates for the CSI imperfections at the cost of BS transmit power.

The impact of different propagation environments is explored in Fig. 10. Rayleigh fading is applicable in dense urban and indoor environments with rich multipath scattering and without a dominant LoS path [67], [69]. Conversely, Rician fading occurs in suburban and rural areas or any scenario with a clear LoS path, like farming, warehouse, and other scenarios [69]. This figure evaluates the transmit power requirements for different Rician factors (κ) for

$$\mathbf{f} = \sqrt{\frac{\kappa}{\kappa+1}}\mathbf{f}^{\mathrm{LoS}} + \sqrt{\frac{1}{\kappa+1}}\mathbf{f}^{\mathrm{NLoS}}, \tag{28a}$$

$$v_k = \sqrt{\frac{\kappa}{\kappa+1}}v_k^{\mathrm{LoS}} + \sqrt{\frac{1}{\kappa+1}}v_k^{\mathrm{NLoS}}, \tag{28b}$$

where $v_k^{\mathrm{LoS}} = 1$ and $\mathbf{f}^{\mathrm{LoS}}$ are the deterministic LoS components between the transmitter and receiver. Also, $\mathbf{f}^{\mathrm{NLoS}}$ and v_k^{NLoS} are the non-LoS (NLoS) components that follow the Rayleigh fading model. Fig. 10 shows high κ factors corresponding to power needs. For example, $\kappa = 2$ and $\kappa = 5$ result in a $3.64\,\%$ and $3.64\,\%$ reduction in transmit power with $M = N = 20$, respectively, when compared to Rayleigh channels. Thus, the LoS component improves the signal power utilization.

VII. Conclusion

This study investigated the concept of ISABC, an innovative system that combines BackCom and sensing. The FD BS plays a dual role; it senses backscatter tag signals while enabling user communication. An algorithm is derived to minimize the BS power consumption by optimizing the BS communication beamformer, sensing signal, tags' reflection coefficients, and the BS sensing combiners. The optimization is subject to communication SINR of targets, EH requirements, and sensing SINR thresholds. The algorithm is based on the AO paradigm and outperforms several benchmarks. The use of tags for sensing and communication opens doors to new possibilities. Future research can explore ISABC channel estimation techniques, waveform/carrier signal design, the signal processing at the BS/tag/reader, key performance indicator development for investigating the communication-sensing performance trade-offs, and state parameter estimation methodologies. Addressing multi-user scenarios, interference mitigation, and practical hardware implementation are also crucial for real-world advancements.

Appendix A
Proof of Theorem 1

Recall the division of (P1) into three sub-problems to optimize sensing combiners $\left(\mathbf{U} := \{\mathbf{u}_k\}_{k=1}^K\right)$, transmit beamformers $(\mathbf{P} = \{\mathbf{w}, \mathbf{S}\})$, and reflection coefficients

$\left(\boldsymbol{\alpha} := \{\alpha_k\}_{k=1}^{K}\right)$ via solving problems (20a), (23a), and (25a), while keeping the other two blocks of variables fixed. Let us define $F(\mathbf{U}, \boldsymbol{\alpha}, \mathbf{P})$ as a function of $\mathbf{U}$, $\boldsymbol{\alpha}$, and $\mathbf{P}$ for the objective value of (19a). First, in step 3 of Algorithm 1 with fixed variables $\boldsymbol{\alpha}^{(i)}$ and $\mathbf{P}^{(i)}$, $\mathbf{U}^{(i+1)}$ is the optimal solution that minimizes the value of the objective function. Accordingly, one finds

$$F(\boldsymbol{\alpha}^{(i)}, \mathbf{U}^{(i+1)}, \mathbf{P}^{(i)}) \leq F(\boldsymbol{\alpha}^{(i)}, \mathbf{U}^{(i)}, \mathbf{P}^{(i)}). \tag{29}$$

Next, in step 4 of Algorithm 1, $\mathbf{P}^{(i+1)}$ is the optimal transmit beamformers with given variables $\boldsymbol{\alpha}^{(i)}$ and $\mathbf{U}^{(i+1)}$ to minimize F via solving (23a). Thus, it guarantees that

$$F(\boldsymbol{\alpha}^{(i)}, \mathbf{U}^{(i+1)}, \mathbf{P}^{(i+1)}) \leq F(\boldsymbol{\alpha}^{(i)}, \mathbf{U}^{(i+1)}, \mathbf{P}^{(i)}). \tag{30}$$

Finally, in step 5 of Algorithm 1 with the given $\mathbf{P}^{(i+1)}$ and $\mathbf{U}^{(i+1)}$, problem (26a) is solved to obtain an optimal solution for $\boldsymbol{\alpha}^{(i)}$, which yields:

$$F(\boldsymbol{\alpha}^{(i+1)}, \mathbf{U}^{(i+1)}, \mathbf{P}^{(i+1)}) \leq F(\boldsymbol{\alpha}^{(i)}, \mathbf{U}^{(i+1)}, \mathbf{P}^{(i+1)}). \tag{31}$$

According to (29)–(31), it follows that [30]:

$$F(\boldsymbol{\alpha}^{(i+1)}, \mathbf{U}^{(i+1)}, \mathbf{P}^{(i+1)}) \leq F(\boldsymbol{\alpha}^{(i)}, \mathbf{U}^{(i)}, \mathbf{P}^{(i)}). \tag{32}$$

For problem (19a), the objective values of Algorithm 1 monotonically decrease with each iteration, always remaining non-negative. This consistency, combined with the design choice where each iteration starts from the previous one's end, ensures the algorithm's convergence. The objective function will decrease or stay the same until it meets the convergence criteria, resulting in a stable solution. Thus, the proof is completed.

REFERENCES

[1] F. Liu, C. Masouros, and Y. Eldar, *Integrated Sensing and Communications*. Springer Nature Singapore, 2023.

[2] W. Zhou, R. Zhang, G. Chen, and W. Wu, "Integrated sensing and communication waveform design: A survey," *IEEE Open J. Commun. Soc.*, vol. 3, pp. 1930–1949, Oct. 2022.

[3] A. Hakimi, D. Galappaththige, and C. Tellambura, "A roadmap for NF-ISAC in 6G: A comprehensive overview and tutorial," *Entropy*, vol. 26, no. 9, Sept. 2024.

[4] "3GPP TR 38.848, Study on ambient iot (internet of things) in RAN, V18.0.0 Rel. 18," Sep. 2023. [Online]. Available: https://portal.3gpp.org/desktopmodules/Specifications/SpecificationDetails.aspx?specificationId=4146

[5] D. T. Hoang, D. Niyato, D. I. Kim, N. V. Huynh, and S. Gong, *Ambient Backscatter Communication Networks*. Cambridge Univ. Press, 2020.

[6] D. Galappaththige, F. Rezaei, C. Tellambura, and S. Herath, "Link budget analysis for backscatter-based passive IoT," *IEEE Access*, vol. 10, pp. 128 890–128 922, Dec. 2022.

[7] F. Rezaei, D. Galappaththige, C. Tellambura, and S. Herath, "Coding techniques for backscatter communications - A contemporary survey," *IEEE Commun. Surveys Tuts.*, pp. 1020–1058, 2th Quart. 2023.

[8] F. Rezaei, C. Tellambura, and S. Herath, "Large-scale wireless-powered networks with backscatter communications—A comprehensive survey," *IEEE Open J. Commun. Soc.*, vol. 1, pp. 1100–1130, Jul. 2020.

[9] R. Long, Y.-C. Liang, H. Guo, G. Yang, and R. Zhang, "Symbiotic radio: A new communication paradigm for passive internet of things," *IEEE Internet Things J.*, vol. 7, no. 2, pp. 1350–1363, Feb. 2020.

[10] Y.-C. Liang, R. Long, Q. Zhang, and D. Niyato, "Symbiotic communications: Where Marconi meets Darwin," *IEEE Wireless Commun.*, vol. 29, no. 1, pp. 144–150, Feb. 2022.

[11] B. Gu, D. Li, H. Ding, G. Wang, and C. Tellambura, "Breaking the interference and fading gridlock in backscatter communications: State-of-the-art, design challenges, and future directions," *IEEE Commun. Surveys Tuts.*, pp. 1–1, 2024.

[12] D. Galappaththige, C. Tellambura, and A. Maaref, "Integrated sensing and backscatter communication," *IEEE Wireless Commun. Lett.*, vol. 12, no. 12, pp. 2043–2047, Dec. 2023.

[13] A. Liu *et al.*, "A survey on fundamental limits of integrated sensing and communication," *IEEE Commun. Surveys Tuts.*, vol. 24, no. 2, pp. 994–1034, 2th Quart. 2022.

[14] J. A. Scheer, Ed., *Principles of Modern Radar: Basic principles*, ser. Radar, Sonar and Navigation. Inst. Eng. Technol., 2010.

[15] D. Galappaththige, S. Zargari, C. Tellambura, and S. Herath, "Dual function of sensing and backscatter communication in cellular networks," *IEEE Internet Things Mag.*, 2024, (Under review).

[16] Z. He *et al.*, "Full-duplex communication for ISAC: Joint beamforming and power optimization," *IEEE J. Sel. Areas Commun.*, vol. 41, no. 9, pp. 2920–2936, Sept. 2023.

[17] "3GPP TSG RAN −97e3, Study on ambient IoT , 9.1 (from RP-222685)," Sept. 2022. [Online]. Available: https://portal.3gpp.org/ngppapp/TdocList.aspx?meetingId=60043

[18] "3GPP TSG RAN Meeting −94e, Study proposal on passive IoT, 8A.1 (from RP-213368)," Dec. 2021. [Online]. Available: https://www.3gpp.org/DynaReport/TDocExMtg–RP-94-e–60214.htm

[19] F. Nassar *et al.*, "Dynamic user clustering and backscatter-enabled RIS-assisted NOMA ISAC," *IEEE Trans. Wireless Commun.*, pp. 1–1, Feb. 2024.

[20] F. R. Ghadi, K.-K. Wong, F. J. Lopez-Martinez, H. Shin, and L. Hanzo, "Performance analysis of FAS-aided NOMA-ISAC: A backscattering scenario," *arXiv*, 2024.

[21] Q. Tao, C. Huang, and X. Chen, "Integrated sensing and communication for symbiotic radio with multiple IoT devices," *IEEE Commun. Lett.*, vol. 28, no. 8, pp. 1820–1824, Aug. 2024.

[22] Z. Zhao *et al.*, "B-ISAC: Backscatter integrated sensing and communication for 6G IoE applications," *arXiv*, 2024.

[23] ——, "Joint beamforming for backscatter integrated sensing and communication," *arXiv*, 2024.

[24] H. Luo, U. Demirhan, and A. Alkhateeb, "ISAC with backscattering RFID tags: Joint beamforming design," *arXiv*, 2024.

[25] J. C. Bezdek and R. J. Hathaway, "Convergence of alternating optimization," *Neural, Parallel Sci. Comput.*, vol. 11, no. 4, pp. 351–368, Dec. 2003.

[26] S. Stanczak, *Fundamentals of Resource Allocation in Wireless Networks Theory and Algorithms*, 2nd ed. Berlin, Heidelberg: Springer Berlin Heidelberg, 2008.

[27] W. Wan, X. Wang, J. Yang, and B. Zhao, "Joint linear pre-coder and combiner optimization for distributed antenna systems," in *Proc. IEEE Global Commun. Conf. (GLOBECOM)*, Dec. 2016, pp. 1–6.

[28] A. M. C. So, J. Zhang, and Y. Ye, "On approximating complex quadratic optimization problems via semidefinite programming relaxations," *Math. Program.*, vol. 110, no. 1, pp. 93–110, Jun. 2007.

[29] Q. Wu and R. Zhang, "Intelligent reflecting surface enhanced wireless network via joint active and passive beamforming," *IEEE Trans. Wireless Commun.*, vol. 18, no. 11, pp. 5394–5409, Nov. 2019.

[30] S. Zargari, S. Farahmand, B. Abolhassani, and C. Tellambura, "Robust active and passive beamformer design for IRS-aided downlink MISO PS-SWIPT with a nonlinear energy harvesting model," *IEEE Trans. Green Commun. Netw.*, vol. 5, no. 4, pp. 2027–2041, Dec. 2021.

[31] X. Wang, Z. Fei, and Q. Wu, "Integrated sensing and communication for RIS-assisted backscatter systems," *IEEE Internet Things J.*, vol. 10, no. 15, pp. 13 716–13 726, Aug. 2023.

[32] M. I. Ismail, A. M. Shaheen, M. M. Fouda, and A. S. Alwakeel, "RIS-assisted integrated sensing and communication systems: Joint reflection and beamforming design," *IEEE Open J. Commun. Soc.*, vol. 5, pp. 908–927, Feb. 2024.

[33] S. Zargari, D. Galappaththige, C. Tellambura, and H. Vincent Poor, "A Riemannian manifold approach to constrained resource allocation in ISAC," *IEEE Trans. Commun.*, pp. 1–1, 2024.

[34] S. Zargari, D. Galappaththige, C. Tellambura, and G. Y. Li, "Downlink beamforming for cell-free ISAC: A fast complex oblique manifold approach," *arXiv*, 2024.

[35] D. Galappaththige, S. Zargari, C. Tellambura, and G. Y. Li, "Near-field ISAC: Beamforming for multi-target detection," *IEEE Wireless Commun. Lett.*, pp. 1–1, 2024.

[36] H. Hua, J. Xu, and T. X. Han, "Optimal transmit beamforming for integrated sensing and communication," *IEEE Trans. Veh. Technol.*, vol. 72, no. 8, pp. 10 588–10 603, Aug. 2023.
[37] D. Galappaththige, F. Rezaei, C. Tellambura, and S. Herath, "Beamforming designs for enabling symbiotic backcom multiple access under imperfect CSI," *IEEE Access*, vol. 11, pp. 89 986–90 005, Aug. 2023.
[38] H. Yang, Y. Ye, K. Liang, and X. Chu, "Energy efficiency maximization for symbiotic radio networks with multiple backscatter devices," *IEEE Open J. Commun. Soc.*, vol. 2, pp. 1431–1444, Jun. 2021.
[39] N. Wu *et al.*, "RIS-assisted integrated sensing and backscatter communications for future IoT networks," *IEEE Internet Things Mag.*, vol. 7, no. 4, pp. 44–50, Jul. 2024.
[40] F. Liu, Y.-F. Liu, A. Li, C. Masouros, and Y. C. Eldar, "Cramér-Rao bound optimization for joint radar-communication beamforming," *IEEE Trans. Signal Process.*, vol. 70, pp. 240–253, Jan. 2022.
[41] M. Mohammadi, Z. Mobini, D. Galappaththige, and C. Tellambura, "A comprehensive survey on full-duplex communication: Current solutions, future trends, and open issues," *IEEE Commun. Surveys Tuts.*, pp. 1–1, 4th Quart. 2023.
[42] M. A. Richards, *Fundamentals of Radar Signal Processing*. McGraw-Hill Education, 2014.
[43] S. Ma, G. Wang, R. Fan, and C. Tellambura, "Blind channel estimation for ambient backscatter communication systems," *IEEE Commun. Lett.*, vol. 22, no. 6, pp. 1296–1299, Jun. 2018.
[44] F. Rezaei, D. Galappaththige, C. Tellambura, and A. Maaref, "Time-spread pilot-based channel estimation for backscatter networks," *IEEE Trans. Commun.*, vol. 72, no. 1, pp. 434–449, Jan. 2024.
[45] D. Wang, F. Rezaei, and C. Tellambura, "Performance analysis and resource allocations for a WPCN with a new nonlinear energy harvester model," *IEEE Open J. Commun. Soc.*, vol. 1, pp. 1403–1424, Sept. 2020.
[46] E. Boshkovska, D. W. K. Ng, N. Zlatanov, and R. Schober, "Practical non-linear energy harvesting model and resource allocation for SWIPT systems," *IEEE Commun. Lett.*, vol. 19, no. 12, pp. 2082–2085, Dec. 2015.
[47] P. Stoica, J. Li, and Y. Xie, "On probing signal design for MIMO radar," *IEEE Trans. Signal Process.*, vol. 55, no. 8, pp. 4151–4161, Aug. 2007.
[48] "Positioning techniques for mobile devices in LTE," Jul. 2015. Available Online: https://www.hsc.com/resources/blog/positioning-techniques-for-mobile-devices-in-lte/.
[49] M. Temiz, E. Alsusa, and M. W. Baidas, "A dual-function massive MIMO uplink OFDM communication and radar architecture," *IEEE Trans. on Cogn. Commun. Netw.*, vol. 8, no. 2, pp. 750–762, Jun. 2022.
[50] S. Abdallah, Z. Verboven, M. Saad, and M. A. Albreem, "Channel estimation for full-duplex multi-antenna ambient backscatter communication systems," *IEEE Trans. Commun.*, pp. 1–1, Mar. 2023.
[51] S. Zargari, C. Tellambura, A. Maaref, and G. Y. Li, "Deep conditional generative adversarial networks for efficient channel estimation in AmBC systems," *IEEE Trans. Mach. Learn. Commun. Netw.*, vol. 2, pp. 805–822, Jun. 2024.
[52] B. Tang and J. Li, "Spectrally constrained MIMO radar waveform design based on mutual information," *IEEE Trans. Signal Process.*, vol. 67, no. 3, pp. 821–834, Feb. 2019.
[53] G. Cui, H. Li, and M. Rangaswamy, "MIMO radar waveform design with constant modulus and similarity constraints," *IEEE Trans. Signal Process.*, vol. 62, no. 2, pp. 343–353, Jan. 2014.
[54] E. F. Knott, *Radar Cross Section Fundamentals*. Boston, MA: Springer US, 1993, pp. 1–26.
[55] U. S. Toro, K. Wu, and V. C. M. Leung, "Backscatter wireless communications and sensing in green internet of things," *IEEE Trans. Green Commun. Netw.*, vol. 6, no. 1, pp. 37–55, Mar. 2022.
[56] H. He, J. Li, and P. Stoica, *Covariance matrix to waveform*. Cambridge University Press, 2012, p. 213–221.
[57] S. Boyd and L. Vandenberghe, *Convex Optimization*. Cambridge, U.K.: Cambridge Univ. Press, 2004.
[58] M. Grant and S. Boyd, "CVX: Matlab software for disciplined convex programming, version 2.1," 2014.
[59] I. P'olik and T. Terlaky, *Interior Point Methods for Nonlinear Optimization*. Berlin, Germany; New York, NY, USA: Springer, 2010.
[60] "3GPP TR 36.814, further advancements for E-UTRA physical layer aspects, V.9.0.0 Rel. 9," Mar. 2010. [Online]. Available: https://portal.3gpp.org/desktopmodules/Specifications/SpecificationDetails.aspx?specificationId=2493
[61] D. Galappaththige, F. Rezaei, C. Tellambura, and S. Herath, "RIS-empowered ambient backscatter communication systems," *IEEE Wireless Commun. Lett.*, vol. 12, no. 1, pp. 173–177, Jan. 2023.
[62] Y. Xu *et al.*, "Energy efficiency maximization in NOMA enabled backscatter communications with QoS guarantee," *IEEE Wireless Commun. Lett.*, vol. 10, no. 2, pp. 353–357, Feb. 2021.
[63] Z. Ni, J. A. Zhang, K. Yang, X. Huang, and T. A. Tsiftsis, "Multi-metric waveform optimization for multiple-input single-output joint communication and radar sensing," *IEEE Trans. Commun.*, vol. 70, no. 2, pp. 1276–1289, Feb. 2022.
[64] F. D. Ardakani, R. Huang, and V. W. S. Wong, "Joint device pairing, reflection coefficients, and power control for NOMA backscatter systems," *IEEE Trans. Veh. Technol.*, vol. 71, no. 4, pp. 4396–4411, Apr. 2022.
[65] A. Al-Nahari, R. Jäntti, D. Mishra, and J. Hämäläinen, "Massive MIMO beamforming in monostatic backscatter multi-tag networks," *IEEE Commun. Lett.*, vol. 25, no. 4, pp. 1323–1327, Apr. 2021.
[66] F. Liu, C. Masouros, A. Li, H. Sun, and L. Hanzo, "MU-MIMO communications with MIMO radar: From co-existence to joint transmission," *IEEE Trans. Wireless Commun.*, vol. 17, no. 4, pp. 2755–2770, Apr. 2018.
[67] S. Zhou and G. Giannakis, "How accurate channel prediction needs to be for transmit-beamforming with adaptive modulation over Rayleigh MIMO channels?" *IEEE Trans. Wireless Commun.*, vol. 3, no. 4, pp. 1285–1294, Jul. 2004.
[68] S. M. Kay, *Fundamentals of Statistical Signal Processing: Estimation Theory*. USA: Prentice-Hall, Inc., 1993.
[69] D. Tse and P. Viswanath, *Fundamentals of Wireless Communication*. Cambridge Univ. Press, 2005.

Shayan Zargari received the B.Sc. degree in Electronic Engineering from Azad University, South Tehran Branch, Tehran, Iran, in 2018, and the M.Sc. degree in Telecommunication Engineering from the Iran University of Science and Technology, Tehran, Iran, in 2020. He is currently pursuing the Ph.D. degree in communications and signal processing at the University of Alberta, Edmonton, AB, Canada.

From 2019 to 2020, he was a visiting researcher at the Electronics Research Institute, Sharif University of Technology, Tehran, Iran, and from 2020 to 2021, he was a visiting researcher at the Department of Electrical and Computer Engineering, Tarbiat Modares University, Tehran, Iran. His research interests include optimization theory, integrated sensing and communication (ISAC), backscatter communication (BackCom), intelligent reflecting surfaces (IRS), unmanned aerial vehicle (UAV) communications, resource allocation in fifth-generation (5G)/six-generation (6G) wireless communication, and green communication. He serves as a reviewer for several IEEE journals, including IEEE JOURNAL ON SELECTED AREAS IN COMMUNICATIONS, IEEE TRANSACTIONS ON COMMUNICATIONS, and IEEE TRANSACTIONS ON WIRELESS COMMUNICATIONS.

Diluka Galappaththige (S'17–M'22) is a post-doctoral research fellow at the Department of Electrical and Computer Engineering, University of Alberta, Canada. He received his B.Sc. degree (First-class honor) in Electrical and Electronic Engineering from the Department of Electrical and Electronic Engineering, University of Peradeniya, Sri Lanka, in 2017, and his Ph.D. in Electrical and Computer Engineering from the School of Electrical, Computer, and Biomedical Engineering, Southern Illinois University, Carbondale, IL, USA, in 2021.

Dr. Galappaththige has been awarded a post-doctoral fellowship from NSERC for the academic year 2024-2026. His current research interests include but are not limited to, the design, modeling, and analysis of massive multiple-input multiple-output (mMIMO) communication (i.e., including co-located mMIMO and cell-free/distributed mMIMO), full-duplex communication (FD), backscatter communication (BackCom), reconfigurable intelli-

gent surfaces (RISs), integrated sensing and communication (ISAC), near-field ISAC, wireless power transfer, and emerging technologies for enabling fifth-generation (5G) and beyond wireless networks. He was a recipient of the Exemplary Reviewer Award for IEEE Wireless Communications Letters (TWCL) in 2020, and IEEE Communications Letters (TCL) in 2021. He has actively served as a reviewer for a variety of IEEE journals and conferences, including IEEE Transactions on Communications, IEEE Internet of Things Journal, IEEE Transactions on Vehicular Technology, IEEE Transactions on Green Communications and Networking, IEEE Access, IEEE Network, IEEE Open Journal of Communications Society, TCL, TWCL, IEEE International Conference on Communications, and IEEE Global Communications Conference.

Chintha Tellambura (Fellow, IEEE) received the B.Sc. degree (First class) in electrical and electronic engineering from the University of Moratuwa, Sri Lanka, the M.Sc. degree in electrical engineering from King's College, University of London, and the Ph.D. degree in electrical engineering from the University of Victoria, Canada. He was with Monash University, Australia, from 1997 to 2002. Dr. Tellambura is a Professor in the Department of Electrical and Computer Engineering at the University of Alberta. He has authored or co-authored over 650 journals and conference papers, demonstrating his expertise in the field. According to Google Scholar, his exceptional scholarly contributions have earned him an impressive H-index of 84. Dr. Tellambura has made significant contributions to various areas of research, including future wireless networks, machine learning for wireless networks, and signal processing.

Recognizing his outstanding accomplishments, he was elected as an IEEE Fellow in 2011 for his noteworthy contributions to physical layer wireless communication theory. In 2017, he was further honored as a fellow of the Canadian Academy of Engineering, a testament to his exceptional achievements. His dedication and expertise have been acknowledged through prestigious awards, including the Best Paper Awards in the Communication Theory Symposium in 2012, the IEEE International Conference on Communications (ICC) held in Canada in 2017, and another ICC in France. Moreover, Dr. Tellambura has been honored with the esteemed McCalla Professorship and the Killam Annual Professorship by the University of Alberta, further underscoring his significant impact on academia. Dr. Tellambura has also played a vital role in editorial responsibilities within the IEEE community. He served as an Editor for the IEEE Transactions on Communications from 1999 to 2011 and for the IEEE Transactions on Wireless Communications from 2001 to 2007. In the latter role, he was Area Editor of Wireless Communications Systems and Theory from 2007 to 2012, contributing to advancing the field through his editorial expertise.